Economic Operational Analytics for Energy Storage Placement at Different Grid Locations and Contingency Scenarios with Stochastic Wind Profiles

Deepak Kumar Panda[1], Saptarshi Das[1,2,*]

1) *Department of Mathematics, College of Engineering, Mathematics and Physical Sciences, University of Exeter, Penryn Campus, Cornwall TR10 9FE, United Kingdom*. (e-mail: dp457@exeter.ac.uk).
2) *Institute for Data Science and Artificial Intelligence, University of Exeter, Laver Building, North Park Road, Exeter, Devon EX4 4QE, United Kingdom*. (e-mail: saptarshi.das@ieee.org, s.das3@exeter.ac.uk).

Phone: +44-7448572598

Abstract:

The placement of energy storage systems (ESS) in smart grids is challenging due to the high complexity of the underlying model and operational datasets. In this paper, non-parametric multivariate statistical analyses of the energy storage operations in base and contingency scenarios are carried out to address these issues. Monte Carlo simulations of the optimization process for the overall cost involving unit commitment and dispatch decisions are performed with different wind and load demand ensembles. The optimization is performed for different grid contingency scenarios like transmission line trips and generator outages along with the location of the ESS in different parts of the grid. The stochastic mixed-integer programming technique is used for optimization. The stochastic model load demand and wind power are obtained from real data. The uncertainty in the operational decisions is obtained, considering the different stochastic realizations of load demand and wind power. The data analytics is performed on ESS operations in the base and its corresponding contingency scenarios with different locations in the grid. Moreover, it is aided by non-parametric multivariate hypothesis tests to understand their dependence amongst various parameters and locations in the grid. The numerical analysis has been shown on a simple 3-bus system considering all the locational and contingency scenarios.

Keywords: energy storage, multivariate hypothesis testing, unit commitment, optimal scheduling, contingency scenario

NOMENCLATURE

Variable and Parameter indexing

Symbol	*Meaning*
i	Index over injection (generation units, storage units and dispatchable or curtailable loads)
j	Index over scenarios
k	Index over post-contingency cases (k= 0) for base case
t	Index time over periods
I	Indices of units (generators units, storage units, and dispatchable and curtailable loads) available for dispatch time t
J	Set of all the scenarios considered
K	Set of all the contingencies considered
T	Set of indices of periods in the planning horizon, typically $\{1,\cdots,k\}$

Optimization Variables

Symbol	*Meaning*
p^{tijk}	Injection of active power for unit i at time t in the post-contingency state k for scenario j.
p_{+}^{tijk}, p_{-}^{tijk}	Upward/downward deviation from active power contract quantity for unit i in the post-contingency state k of scenario j at time t.
$\delta_{+}^{ti}, \delta_{-}^{ti}$	Upward/downward load following ramping reserves needed from unit i at time t for the transition to time $t+1$.
u^{ti}	Binary commitment state for unit i in period t, 1 if the unit is online, 0 otherwise.
v^{ti}, w^{ti}	Binary startup and shutdown states for unit i in period t, 1 if the unit has a startup/shutdown event.

p_{sc}^{tijk} , p_{sd}^{tijk}	Charge/discharge power injections of the storage unit i in the post-contingency state k of the scenario j at time t.
s_0^i	Expected stored energy in the storage unit i.
r_+^{ti} , r_-^{ti}	Upward/downward contingency power provided by the reserve i at time t.
s_+^{ti} , s_-^{ti}	Endogenously computed upper/lower bounds for the unit i on the energy stored at the end of period t. For $t=0$, this is a fixed input parameter representing the bounds at the beginning of the first period.
τ_i^+ , τ_i^-	Minimum up and downtime for unit i for the number of periods.

Constraint Functions and Parameters

Symbol	*Meaning*
$g^{tjk}(.)$	Nonlinear AC power flow equations in post-contingency state k of the scenario j at time t
$h^{tjk}(.)$	Transmission voltage and other limits in the post contingency state k of scenario j at time t.
$R_{\max+}^{ti}$, $R_{\min+}^{ti}$	Upward/downward contingency reserve capacity limits for the unit i at time t.
$\Delta_{\max+}^{ti}$, $\Delta_{\min+}^{ti}$	Upward/downward physical ramping limits for the unit i for the transition from the base $k=0$ to contingency cases.
$S_{\max+}^{ti}$, $S_{\min+}^{ti}$	Stored energy (in MWh) max/min limits for the storage unit i at the end of the final period n_t .
$S_{\min}^{0i}$, $S_{\max}^{0i}$	Lower/upper bound on the initial stored energy in storage unit i.
$S_{\min}^{n_t i}$, $S_{\max}^{n_t i}$	Lower/upper bound on the initial stored energy in storage unit i at the end of the period n_t .
$P_{\min}^{tijk}$, $P_{\max}^{tijk}$	Limits on the active injection of unit i in post-contingency state k of scenario j at time t.

Cost Functions and Parameters

Symbol	*Meaning*
$f_p(.)$	The total energy cost for delivery.
$f_{\text{lf}}(.)$	Load following costs by the energy storage and generator reserves.
$f_{\text{uc}}(.)$	Unit commitment cost.
$f_s(.)$	Energy storage operational cost
$C_P^{ti}(.)$	The cost function for active injection i at time t.
$C_{P+}^{ti}(.), C_{P-}^{ti}(.)$	Cost for upward/downward deviation of active power contract quantity from unit i at time t.
$C_{R+}^{ti}(.), C_{R-}^{ti}(.)$	Cost of upward/downward contingency reserve purchased from unit i at time t.
$C_{\delta_+}^{ti}(.), C_{\delta_-}^{ti}(.)$	Cost of upward/downward load following reserve for the unit i at time t.
C_{s0}	The cost associated with the storage for starting with a given level of stored energy s_0 in the storage unit at the time $t=0$
C_{ts0}	The cost associated with the storage for starting with a given level of stored energy s_0 in the storage unit at time t in the multi-period optimization.
C_{sck} , C_{sdk}	Vector of prices by the storage unit for contribution to terminal storage from charging/discharging at the end of the contingency state.
C_{sc0} , C_{sd0}	Vector of prices by the storage unit for contribution to terminal storage from charging/discharging at the end of the base state.
C_v^{ti} , C_w^{ti}	Startup and shut down costs for the unit i at time t.

Other Parameters

Symbol	*Meaning*
Δ	Length of scheduling time in hours, 1 hour is considered here.
η_{in}^{ti} , η_{out}^{ti}	Charging/discharging efficiencies for the storage unit i at time t.
η_{loss}^{ti}	The fraction of storage energy lost per hour by the unit i at time t per startup/shutdown cost.
α	The fraction of the time slice that is spent in the base case before the contingency occurs.

ψ_0^{tijk}	Conditional probability of contingency for the contingency state *k* scenario *j* and time *t*.
γ^t	Probability of making into period *t* without branching off the central path in the contingency period $\{1,\ldots,t-1\}$.
s_I^{tij0}	Vector of expected stored energy for the storage unit *i* scenario *j* at the start of period *t* without any contingency scenario.
s_I^{tijk}	Vector of expected stored energy for the storage unit *i* scenario *j* and post contingency state *k* at start of period *t* without any contingency scenario.
s_Δ^{tij0}	Net increase in stored energy due to charging and discharging of storage unit *i* for scenario *j* at time *t*
s_Δ^{tijk}	Net increase in stored energy due to charging and discharging of storage unit *i* for scenario *j* and post contingency state *k* at time *t*
s_F^{tij0}	Vector of expected stored energy for the storage unit *i* scenario *j* at the end of period *t* without any contingency scenario.
s_F^{tijk}	Vector of expected stored energy for the storage unit *i* scenario *j* post contingency state *k* at the end of period *t* without any contingency scenario.
s_α^{tijk}	Expected stored energy for the storage unit *i* scenario *j* and contingency *k* occurring at a probability α.

1. INTRODUCTION

The deployment of ESS in modern power systems and smart grids has been experiencing rapid growth. It provides a solution to mitigate volatility and intermittency in wind energy, meeting real-time demands, thus improving its reliability and economy as discussed in [1]. There have been many successful deployments of bulk energy storage in smart power grids [2], [3]. As shown in [4], energy storage can provide other benefits to the power grids. These include robustness of the network sizing during peak periods and eliminating grid reinforcements with renewable energy integration, thus improving the stability of the power system. Several examples of battery storage deployments with wind energy systems have been discussed in [5]. ESS is operated as a generator and a load in case of grid under-voltage and over-voltage conditions. Thus ESS operations involve different stakeholders based on the benefits it provides to the whole electricity systems as discussed in [6], [7]. It provides flexible features in the grid-like supply and reserve sharing, demand flexibility, variable generation curtailment, the addition of new loads, and grid specific applications such as power quality, balance, and overall management. However, the placement of energy storage devices in the right location of the grid is essential as it provides several market and operational benefits. The effects and previous works on the ESS placement in the grids are explained in the next sub-section.

1.1. Previous Works on Energy Storage System Placement and Sizing

The sizing and placement of ESS play an essential role in power grid operations. As shown in [8], [9], the energy loss reduction, and the voltage improvement of the nodes are affected by the location of the energy storage devices. ESS also helps in reduction of energy loss and environmental emissions, promotion of energy arbitrage, deferral in network upgrade, and providing reactive power support as shown in [10]. The work in [11] suggests that inappropriate location of energy storage devices in the grid affects the reliability of the grid, influencing the grid frequency and voltage stability.

There have been several joint optimization approaches for the placement of distributed generators (DG) and ESS. In [12], installation locations are obtained using a loss sensitivity approach (LSF) by solving a two-stage optimization problem. The first stage deals with the location of the DG in the grid while the second stage finds the optimal capacity. The ESS capacity is found using chance-constrained programming. In [13], coordinated ESS and DG planning are performed, incorporating active and reactive power. The problem is framed as a mixed-integer programming problem. It is solved using particle swarm optimization (PSO) and meta-heuristic techniques. The design variables for optimization are active and reactive power capacities of DG and ESS, for improving the overall grid voltage profile. Generally, the power grid operational cost or the performance is selected as a suitable criterion for solving the sizing and placement problems of ESS. Dynamic models of the power grid have also been used for the placement of ESS to improve the transient performance of the power grid.

The optimization approach involving operational cost is adopted in [14]–[21]. In the given problem, binary decision variables are used for obtaining the location of ESS in the grid. Here the optimization is generally divided into two stages where the location is found out in the first stage, and the capacity of the ESS and the operational

strategies are found in the second stage. In [21], the optimal mix of ESS and the size of an on-load tap changing transformer (OLTC) is utilized to minimize the capital investment and operational costs. Nonconvex constraints are linearized using the Big-M method, and a second-order cone programming is used to solve the optimization problem. Joint optimization incorporating ESS and OLTC provided better operation in terms of frequency regulation, energy arbitrage, and congestion management. In [20], the ESS placement problem is solved with high photovoltaic (PV) penetration by minimizing the energy losses and environmental emissions along with optimizing energy arbitrage, transmission access fee, capital, and maintenance cost, which are translated into economic benefits with operational constraints. In [17], the optimization is performed considering the number of batteries as constraints. In [18], minimization of energy loss is considered along with the idle commitment status of ESS along with charge and discharge variables. The number of batteries has been used as constraints for solving the optimization problem. The operational strategies are obtained, considering the same initial and terminal state. In [17], stochastic mixed-integer linear programming (MILP) has been used to minimize the overall investment and operational cost, which includes the capital cost of deployment, penalty cost incurring due to the DG spillage, marginal cost, and capacity of DG. Various constraints involved in decision making are the operational, intertemporal, binary variable for start-up and shutdown for conventional generators, generation, and network dispatch, and nodal power balance. In [22], the solar irradiance prediction using autoregressive integrated moving average (ARIMA) model has been utilized in the MILP problem. The total installation and inverter capacity cost is optimized. Under-voltage and over-voltage, along with maximum and minimum state of charge (SOC) constraints, are considered for the battery ESS. The overall objective was the maximization of the self-consumption where the distributed network operator (DNO) and third-party operator pays for the installation and operational cost for battery energy storage system (BESS) respectively.

Due to the presence of the nonlinear convex constraints the optimization problems have been solved using swarm and evolutionary optimization techniques in [15], [19], [23]. An artificial neural network (ANN) is used in [14] to improve the predictability of the wind power plant operations. It also helps finding the optimal size of the ESS to reduce the cost associated with the operation of energy reserves. The prediction is incorporated into the optimization problem. It is solved using the gray wolf optimization technique in [19], considering the cost-benefit analysis of the optimal sizing of the ESS in the microgrid. The uncertainties of wind turbine and fuel cell operation in the microgrid are considered in the two-stage randomization step. The prediction error caused due to wind power uncertainty is considered as the random variable in the optimization problem. In [23], the whale optimization technique is used for finding the optimal positioning and energy storage sizing, which is found in a two-stage process. The performance is benchmarked with the firefly and PSO algorithm. The analysis was conducted considering a single battery and multiple batteries of high and low capacities, respectively. It is observed that the system performance was better in the former case. Fuzzy PSO is used in [15] to maximize the profit of the distribution company (DISCO). Optimal operating conditions are obtained by the placement of ESS based on the energy acquisition mode. Locational margin price (LMP) is considered for the economic cost involved with the DISCO.

Fast model predictive controller (MPC) is used in [24] for finite horizon online optimization. It is used to determine the location of ESS while optimizing the overall cost as shown in [25]. The problem is solved in two stages. In [25], economic MPC (EMPC) is utilized to find the ESS's optimal placement configuration. ESS sizing and placement problem is solved in the first stage using economic linear optimal control with non-relaxed constraints. Gradient search techniques using EMPC are utilized to find optimal storage operations in the second stage of the problem. Receding horizon MPC is utilized in [26] for solving sizing and placement problems for the distributed ESS. Multi-period optimal power flow (OPF) is utilized to solve the placement problem, and investment analysis is also conducted along with it. The utilization of the PV is also incorporated in the optimization problem and along with ESS degradation cost. Probabilistic constraints signify the forecast errors so that the stochastic optimization can be performed without sampling-based approaches. This allows simulation of the wide range of scenarios and errors. In addition to this, inter-temporal constraints for ESS is also considered. The battery degradation cost is a function of battery power and state of charge of the device and incorporated as an epigraph of convex piecewise affine functions. Similarly, the probabilistic constraints were also formulated in [27], considering the forecast errors to solve the two-stage stochastic programming through MPC along with the chance constraints.

Voltage [28] and time-domain [29] system performance has been utilized for the placement and sizing of ESS. In [28], ESS has been optimally allocated, considering the optimized voltage deviation, flicker, power loss, and line loading. The optimal placement of the ESS has been analysed with respect to improvements in power

quality. Fitness scaled chaotic artificial bee colony optimization has been used to find the resulting decision variables. The voltage flicker minimization is achieved through ESS operational strategies. Optimal sizing of ESS to prevent under and over-voltage fluctuations has been discussed in [30]. The optimization is performed in two stages where the sizing problem is solved in the first stage, and the operational problem under uncertain load demand and DG is solved in the second stage. Multi-period optimization is considered with different scenarios while exploiting the structure of the algorithm. The dispatch strategies are obtained using AC-OPF in the second stage of the optimization.

In [31], multi-period OPF is solved with relaxed constraints on the number, location, and size of the ESS used in the grid. Voltage sensitivity is utilized to determine the location of ESS. Power system oscillations damping were considered for the ESS placement in [29]. Here, ESS is modelled using a second-order model used for describing synchronous generator operation and dynamics. It represents the virtual inertia of the DG present in the grid. The virtual inertia helps attain the optimum frequency stability of the grid. The dynamical system performance metrics were used along with the cost of the optimization problem. In [32], the optimization problem involves system controller tuning and placing the ESS in the grid. The power converter is modelled considering the time constants, SOC, and power limits. The optimization is solved using a black-box mixed-integer technique, which is interfaced with the time-domain simulations. The optimization constraints were put on the number of ESS devices along with the threshold of power system performance. The mixed-integer PSO technique was found to be robust against seasonal load changes. Microgrid structure-preserving energy function was designed and utilized using internal potential energy in [33], for obtaining optimal ESS placement. Energy function models the transient stability of the microgrid. The economy of the system is sacrificed for faster recovery and lesser overshoot.

The multi-objective optimization strategy for placement and sizing of ESS considering the grid's operational performance and the economy is solved using stochastic optimization to reduce the overall investment, operation, and maintenance and battery lifetime degradation costs. The budgetary and location constraints, along with operational constraints like reverse power flow, wind and solar power output, transformer tappings, and capacitor banks, were used while solving the problem. Chance constraints have been utilized for different load decompositions considering conservative voltage reductions. The trade-off between economic and technical goals are achieved in [16]. Operational goals involve voltage deviation, feeder line congestion, and network losses while the economic goals involve the cost of supplying loads, investment and maintenance costs, load curtailment, and stochasticity of the loads and renewable energy generations. The convex constraints were used to solve the optimization problem using the second-order cone programming method with multiple scenarios generated from data clustering. Five-year time span is considered in the analysis.

The effect of ESS placement in the distribution, and user side is mentioned in [11]. At the generation and distribution side, the ESS helps store the energy during the off-peak period and discharging it during the high demand period [35]. It also aids in seasonal energy storage for long term shifting along with smoothing of the renewable energy output fluctuations [36], where the ramping capacity of the ESS plays an important role. ESS also plays an essential role in the voltage control support for a wind-based system since the latter require reactive power for operation [37]. In addition to this, it also provides support to the grid in renewable energy integration into the grid, replacing the spinning reserve [38] and in various grid outages [37], [38]. When connected to the end-user side, ESS helps in supplying the backup for the power supply system during the short power outages as discussed in [35]. However, a detailed analysis of the ESS operation at the generator end and the user end is not analysed with the grid's overall operation. Security-constrained unit commitment (SCUC), considers planning and operation of the power grid considering different contingency scenarios. The relevant works on SCUC are described in the next subsection.

1.2. Previous Works on Security Constrained Unit Commitment

Security constrained unit commitment or SCUC is generally used to schedule the power dispatch for the controllable energy sources during grid contingencies is shown in [39]. The algorithm is flexible enough to incorporate the changes in system network configurations for contingency. On occasions, the algorithm fails to converge due to violations of AC network constraints at steady and contingency states. Then, Benders mismatch cuts are used in [40] to shed local loads. The forced outage of the generation units, transmission lines, and load forecasting uncertainties are incorporated in [41], where it is modelled as a Markov process. Scenario reduction techniques have been used to model the given outages to make the computation feasible for large scale systems. Deterministic SCUC is solved under each scenario by dividing the problem into several sub-problems. The load

forecasting errors were dealt with using scenario trees. Weighted average generation cost is minimized, considering outages and forecast errors using Lagrangian relaxation techniques to deal with coupled constraints. This work is further extended to incorporate wind power in the SCUC algorithm in [42]. Forecasted wind power is considered in the normal situation, and the unit commitment problem is solved in the master stage of the optimization. Mismatched wind power from the simulated data is considered as a contingency scenario and the algorithm is framed to create a trade-off between the security and economy with the day ahead operations. Non-wind units with ramping capability are used for the dispatch, and the forecasting error is handled accordingly. The uncertainty of wind power is scheduled using response sets in [43]. Response sets are an excellent way to ascertain the availability of the capacity without the stochastic model. SCUC is solved considering the uncertainty of the load demand and wind power in [44], [45], [46]. Also, ramping and spinning reserves are used for the mitigation of the uncertainties of wind and load demand. The point estimate method (PEM) is used to reduce the number of scenarios for the uncertainty. Moreover, it helps in avoiding the under-estimation of flexible resources. Linearized AC network constraints are used for solving the optimization problem.

Wind uncertainty can cause under or over estimation of the spinning reserve usage, while joint scheduling makes it robust against the extreme and probable scenarios. In [46], the SCUC problem is solved considering auto-correlated load demand and wind power generation and random transmission line outages. The reliability of the circuit breaker (CB) considering the number of operations is incorporated in the SCUC problem in [47]. The reliability of CB affects the load shedding. The nonlinearity of the switching operation of CB is linearized and incorporated into the SCUC problem, which limits the number of transmission switching. Dynamic thermal load rating of the transmission line is suggested for the estimation of the system's losses. Due to the high number of transmission lines switching, reliability of the CB becomes less. Switching increases the chances of transmission line outage.

Incorporating ESS in SCUC problems have been performed in [45], [48], [49], [50], [51]. Distributed batteries have been utilized to reduce the overload in the grid in [48]. The algorithm takes advantage of the difference between short-term and long-term loading ratings for transmission lines. The difference is used in taking multistage corrective security constrained optimal power flow (SCOPF) decisions. The decisions activate the energy storage devices to relieve transmission lines of the congestion. Charging and discharging decisions are taken to ensure economic grid operations, and some energy is reserved for post-contingency scenarios. The lithium-ion battery model is modelled in [45] to solve the SCUC problem using the information decision gap theory. The battery degradation cost is used in the objective function to solve SCUC, where information gap decision theory is used to model wind farms and electric vehicles. The wind and load power uncertainties are used as a bi-objective model to deal with the uncertainties faced by the independent system operator (ISO). By tolerating a higher operating cost, higher uncertainty can be accommodated. Multi-objective optimization is used to maximize the uncertainty parameters so that the optimum operating cost is obtained. The energy storage for multi-period optimization, along with inter-temporal constraints, is modelled in [49], where the compressed air energy storage (CAES) is taken into consideration. The compression and expansion of CAES are analogous to the charging and discharging of battery operations. Peak-load reduction, decrease in the system operating cost, and emission and improvement in system reliability commitment have been achieved using CAES. In [50], pumped-storage hydroelectric plants are used for SCUC with high wind energy penetration. Comparison and analysis of fixed-speed and adjustable speed plants are used. Weibull distribution is used to sample the wind power generation in the optimization problem. The analysis is also considered with the inclusion of increasing penetration of wind power. The difference in the operational structure of both plants has been considered in the linearized SCUC model.

The pumped hydroelectric energy is shown to reduce the overall cost of the curtailed wind energy. In [51], the SCUC problem is solved, considering the ESS for transmission line expansion. The MILP problem was divided into master and slave subproblems. Security constraints are not considered in the master problem, where the sum of the investment cost is optimized for the new facilities. While for the sub-problems, corrective control during the post contingency is considered to minimize the risk costs. The outage of the transmission line is considered with ESS, thus defining a shared responsibility between the ESS owners and the transmission line operators. Allocation cost is analysed with the placement of energy storage on a different bus. Considering the operation, investment, and risk costs, ESS can provide power to the local loads and absorb the excess power from the intermittent energy sources. Hence the location of energy storage is critical. Its power dispatch is found by solving mixed-integer linear programming techniques with $(N-1)$ reliability criterion, where N represents the possible set of contingencies. The contingencies are modelled as a stochastic optimization based SCUC problem

in [53] with energy storage. The optimization model involves incorporating the reserves as a part of the energy source during contingency scenarios. However, in [53], a detailed energy storage model is not considered in the optimization process. The model also does not involve Markov modelling of wind power as a part of the uncertainty. The work in [3] combines the detailed battery storage constraint model as a part of the stochastic unit commitment problem. In this problem, the contingency scenarios are considered as probabilistic. Two types of uncertainties are tackled in this paper – the first is wind power, which is modelled as a sequence of scenarios. In the second case, discrete events such as line or generator tripping (α) , which represents the fraction of the time, the system is in the base state, before branching off to contingency state.

1.3. Contributions of This Paper

As compared to existing literature, the work reported in this paper analyses the energy storage operation at different locations in the grid. It combines the problem of SCUC and the placement of ESS in different grid locations. The analytics is focused mostly on the placement of ESS near the load, thermal generation, or wind power generation with the operational effects defined in [11]. However, the contingency effects on ESS operations are not mentioned and not worked upon much in recent literature. The contingency cases are carried out by extending the research reported in [3] to incorporate the fraction of time slice before contingency (α) in the energy storage model, along with its inter-temporal constraints as defined in [26]. The energy storage operations during several contingencies, along with their location on several buses in the grid, have been analysed along with the base case scenarios. The operational analytics of the ESS is considered with respect to the economical running cost. The wind power forecasting error is modelled from the real-world data using Markov chains. The real-world load demand patterns are also used in the optimization problems during the Monte Carlo simulations. Hence, with the consideration of the ESS storage operations, while optimizing the total system cost along with real wind power and load demand patterns incorporating a variety of system contingencies, makes the problem very practical. The analysis is based on the ESS operational model, which is derived from the contingency scenarios of the grid. It also causes a relative change of the minimum and maximum energy that can be stored, which is reflected in the inter-temporal constraints of the ESS. These constraints, along with the charging and discharging models, play an essential role in the operation based with different location in the grid.

The similarity in base and contingency operational states are quantified by non-parametric multivariate statistical tests of the storage operations. Non-parametric multivariate statistical tests are widely used in various other interdisciplinary research fields. It includes analysis of the assessment of completers and non-completers in massive open online courses in [54], soil sample in [55], gene expressions of different parts of the brain with schizophrenia [56]. It is also used to study the influence of minimal access surgery techniques on the patients having different body mass index in [57], and decrease in cognitive load during reading and comprehension using automatic layout management interface in [58]. The cognitive load metrics are analysed using Wilks lambda test statistic.

Furthermore, this is the first work, where Monte Carlo simulations of different realization of the wind power and load demand uncertainty are conducted on multiperiod optimization problems for different contingency scenarios. In previous works, contingencies and storage placement is studied concerning the operation of the power grid. However, in this paper, the operation of the storage is compared and analysed concerning different contingencies and locations in the grid. Moreover, the operations are also compared with the base conditions at different contingency scenarios. This is obtained due to the probabilistic weighting of the base and contingency states in the objective function. Non-parametric statistical analysis was conducted on the operational data obtained with different simulation ensembles of wind power and load demand to determine the ESS operational similarity for different contingency scenarios when it is placed at different locations in the grid. The operation was carried out on a small 3-bus system since, with the increase in scenarios, the computational burden will increase and cause ill-conditioned results as discussed in [30].

The analysis was conducted considering a range of grid contingency scenarios. As compared to the previous works, the main contributions and novelty of this paper are as follows:

- The wind and load power are modeled from real dataset in an appropriate form for performing the stochastic optimization algorithm for the solver.
- An analytical study is conducted comparing the nature of storage operations in base and contingency states.
- A detailed study is conducted on the ESS operations obtained from the unit commitment algorithm under base conditions with the energy storage placed at different locations in the grid.

- The similarity in base and contingency operational conditions is found from different locations of the energy storage in the grid using non-parametric multivariate hypothesis tests.

2. PROBLEM FORMULATION

The scheduling of the generators as a multi-period optimization can be formulated as a unit commitment problem along with economic dispatch. Here the objective is to minimize the overall cost, considering the operational costs of the generator and energy storage devices. The stochastic optimization is formulated considering the uncertainty of wind power in multiple time steps. The multi-period stochastic optimization problem is solved at each time instant considering all the inter-temporal constraints.

The optimization problem and modelling are formulated based on the functionalities of the MATPOWER Optimal Scheduling Tool (MOST) as given in [3], [59]. The problem is solved using mixed-integer programming, which takes the stochastic input in the form of wind power. The wind power is modelled in the form of scenarios from the real data. The statistical model of load demand is formulated from the real data. Random samples of the load demand are used in the Monte Carlo simulation of the optimization problem. The transition probability matrix is used to define the Markov switching between the wind power states for various periods. The transition probability matrix is used as a random variable for each Monte Carlo ensemble. The overall scheme of statistical modelling, optimization, and analytics is shown in Figure 1. The MOST solver provides hourly unit commitment decisions for the generators, energy storage device, and dispatchable loads connected to the grid. The mathematical structure of the cost function for optimization, constraints, and energy storage operations, along with the stochastic variables, are presented in the following subsections.

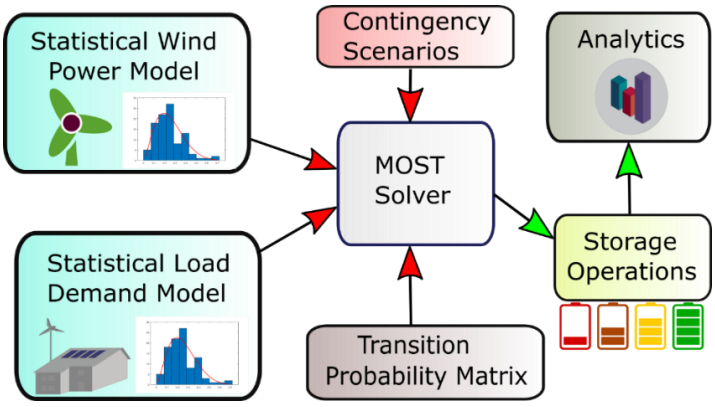

Figure 1. Operational scheme for generating operational ESS values from the stochastic load and wind power model along with various contingency scenarios.

2.1 OBJECTIVE FUNCTION FORMULATION

The multiperiod mixed-integer stochastic programming is based on the concept of making optimal decisions based on the data available at that time, where the algorithm is generally solved in two steps given as:

$$\min_x \left\{ g(x) = f_{\text{det}}(x) + \mathbb{E}_{\xi}\left[Q(x,\xi) \right] \right\}. \tag{1}$$

The constraints on x, solved in (1) given as $Tx \le h$, is incorporated in the second part of the problem, where $Q(x,\xi)$ is the optimal value obtained by solving:

$$\min_y \left\{ q(y,\xi) | T(\xi)x + W(\xi)y = h(\xi) \right\}. \tag{2}$$

Thus, $x \in \mathbb{R}^n$ is the first stage decision variable while $y \in \mathbb{R}^m$ represents the second stage decision variables. Here, $f_{\text{det}}(x)$ and $\xi(q,T,W,h)$ represent the deterministic and the stochastic part of the objective function, respectively. $\mathbb{E}[\cdot]$ represents the expected value of the stochastic component of the objective function. In the case of SCUC problem, x represents the commitment status for the controllable generation sources found by solving $g(x)$ in (1) while y represents the power dispatch of the controllable generators found by solving (2).

Since this is a multi-period optimization problem, we expect the optimization to be solved using the methodology described in (1) and (2). The optimization decision variables are subjected to inter-temporal constraints. The total objective function for optimization can be written as:

$$\min f(x) = f_p(p, p_+, p_-) + f_{1f}(\delta_+, \delta_-) + f_{uc}(u, v, w) + f_s(s_0, p_{sc}, p_{sd}). \tag{3}$$

The objective functions can be defined as follows:

- *Generation Costs*: The generation costs are considered as a quadratic polynomial of the generation quantity, which is modelled using the stochastic variables as:
$$f_p(p, p_+, p_-) = \sum_{t\in T}\sum_{j\in J^t}\sum_{k\in K^{tj}} \psi_\alpha^{tjk} \sum_{i\in I^{tjk}} C_P^{ti}(p^{tijk}) \,. \tag{4}$$
- *Load Following Reserve Costs*: The costs involved in maintaining the balance between the total generation and demand by scheduling the storage and the generator reserves during the given time interval can be written as:
$$f_{lf}(\delta_+, \delta_-) = \sum_{t\in T}\gamma^t \sum_{i\in I^t}\left[C_{\delta+}^{ti}(\delta_+^{ti}) + C_{\delta-}^{ti}(\delta_-^{ti})\right]. \tag{5}$$
- *Unit Commitment Costs*: The costs due to the startup and shutdown of the generation units can be written as:
$$f_{uc}(u, v, w) = \sum_{t\in T}\gamma^t \sum_{i\in I^t}\left(C_P^{ti}(0)u^{ti} + C_v^{ti}(0)v^{ti} + C_w^{ti}(0)w^{ti}\right). \tag{6}$$
- *Storage Operations Costs*: The cost of the initial, terminal stored energy and leftover energy in the terminal states is:
$$f_s(s_0, p_{sc}, p_{sd}) = \sum_{i\in I^{tjk}} C_{s0}^T s_0^{\,i} - \sum_{t\in T}\left(C_{s0}^T s_{0t}^{\,i} + \sum_{j\in J^t}\sum_{k\in K^{tj}} C_{sc}^T p_{sc}^{\,tijk} + C_{sd}^T p_{sd}^{\,tijk}\right). \tag{7}$$

2.2 CONTINGENCY CONSTRAINTS FORMULATION

The following equations define the operational constraints on the storage that act as reserves during contingency like generator trips or transmission line failure. The total limit on the reserve, redispatch and contract variables are:

$$\begin{aligned} &0 \le p_+^{tijk} \le r_+^{ti} \le R_{max+}^{ti}\,, \\ &0 \le p_-^{tijk} \le r_-^{ti} \le R_{max-}^{ti}\,. \end{aligned} \tag{8}$$

Ramping limits due to the contingency operations can be defined as:

$$-\Delta_{\max-}^{i} \le p^{tijk} - p^{tij0} \le \Delta_{\max+}^{i}, \quad k \ne 0. \tag{9}$$

2.3 RESIDUAL ENERGY STORAGE CONSTRAINTS

(1) Base Case Scenario

It is essential to compute the expected amount of stored energy s_F^{tij0} for the unit i at the end of the period t in the base state j. The losses are proportional to the average stored energy during the period. The process is to be represented as:

$$\begin{aligned} s_F^{tij0} &= s_I^{tij0} + s_\Delta^{tij0} - \Delta\eta_{loss}^{ti}\frac{s_I^{tij0} + s_\Delta^{tij0}}{2}, \\ &= \beta_1^{ti} s_I^{tij0} + \beta_1^{ti} s_\Delta^{tij0}, \end{aligned} \tag{10}$$

$$\text{where, } \beta_1^{ti} \equiv \frac{1-\Delta\eta_{loss}^{ti}/2}{1+\Delta\eta_{loss}^{ti}/2}\,,\ \beta_2^{ti} \equiv \frac{1}{1+\Delta\eta_{loss}^{ti}/2}\ \text{, and } s_\Delta^{tijk} \equiv -\Delta\left(\eta_{\text{in}}^{i} p_{sc}^{tijk} + \frac{1}{\eta_{out}^{i}} p_{sd}^{tijk}\right). \tag{11}$$

The total operational power from the storage is the net power used for charging and discharging:

$$p^{tijk} = p_{sc}^{tijk} + p_{sd}^{tijk}\,, \tag{12}$$

where,

$$p_{sc}^{tijk} \le 0,\ p_{sd}^{tijk} \ge 0. \tag{13}$$

Charging power is considered negative and discharging power as positive. The charging and discharging energy of the storage device should be operated within the following limits:

$$s_{-}^{ti} \geq S_{\min}^{ti}, \quad s_{+}^{ti} \leq S_{\max}^{ti}. \tag{14}$$

The change in the stored energy per horizon during charging and discharging period can be represented as:

$$\begin{aligned} s_{-}^{ti} &\leq s_{-}^{(t-1)i} + s_{\Delta}^{tij0} - \Delta \frac{\eta_{loss}^{i}}{2}\left(s_{-}^{ti} + s_{-}^{(t-1)i}\right), \\ s_{+}^{ti} &\geq s_{+}^{(t-1)i} + s_{\Delta}^{tij0} - \Delta \frac{\eta_{loss}^{i}}{2}\left(s_{+}^{ti} + s_{+}^{(t-1)i}\right). \end{aligned} \tag{15}$$

(2) Contingency Scenario

When the contingency occurs at a fraction α , the expected stored energy can be computed as follows:

$$s_{\alpha}^{tijk} = s_{I}^{tijk} + \alpha\left(s_{F}^{tij0} - s_{I}^{tij0}\right). \tag{16}$$

The losses occurred in the storage can be computed as:

$$s_{loss}^{tijk} = \Delta\eta_{loss}^{ti}\left[\alpha\frac{s_{I}^{tijk} + s_{\alpha}^{tijk}}{2} + (1-\alpha)\frac{s_{I}^{tijk} + s_{F}^{tijk}}{2}\right]. \tag{17}$$

The final stored energy is given as:

$$s_{F}^{tijk} = s_{i}^{tijk} + \alpha s_{\Delta}^{tij0} + (1-\alpha)s_{\Delta}^{tijk} - s_{loss}^{tijk}. \tag{18}$$

Substituting the values obtained in (16) and(17), we get:

$$s_{F}^{tijk} = \beta_{5}^{ti} s_{I}^{tijk} + \beta_{4}^{ti} s_{\Delta}^{tij0} + \beta_{3} s_{\Delta}^{tijk}. \tag{19}$$

where,

$$\beta_{3}^{ti} \equiv \left(\frac{1}{1-\alpha} + \Delta\frac{\eta_{loss}^{ti}}{2}\right)^{-1} = \frac{1-\alpha}{1+(1-\alpha)\Delta\eta_{loss}^{ti}/2}, \tag{20}$$

$$\beta_{4}^{ti} \equiv \frac{\alpha}{1-\alpha}\beta_{2}^{ti}\beta_{3}^{ti} = \frac{\alpha}{\left(1+\Delta\eta_{loss}^{ti}/2\right)\left(1+(1-\alpha)\Delta\eta_{loss}^{ti}/2\right)}, \tag{21}$$

$$\beta_{5}^{ti} \equiv \frac{\beta_{1}^{ti}}{\beta_{2}^{ti}}\left(\beta_{3}^{ti} + \beta_{4}^{ti}\right) = \left(1-\Delta\eta_{loss}^{ti}/2\right)\frac{\alpha + (1-\alpha)\left(1+\Delta\eta_{loss}^{ti}/2\right)}{\left(1+(1-\alpha)\Delta\eta_{loss}^{ti}/2\right)\left(1+\Delta\eta_{loss}^{ti}/2\right)}. \tag{22}$$

The constraints related to the minimum and maximum energy injection conditions can be described as:

$$\begin{aligned} s_{min}^{ti} &\leq s_{-}^{(t-1)i} + \alpha s_{\Delta}^{tij0} + (1-\alpha)s_{\Delta}^{tijk}, k \neq 0, \\ s_{max}^{ti} &\geq s_{+}^{(t-1)i} + \alpha s_{\Delta}^{tij0} + (1-\alpha)s_{\Delta}^{tijk}, k \neq 0. \end{aligned} \tag{23}$$

The model of the energy storage operation described in (19), highlights its operational aspect when the grid is under contingency. This is also reflected in the minimum and maximum energy that can be stored along with the charging and discharging energy in the given time period as shown in (23).

2.4 UNIT COMMITMENT CONSTRAINTS

The unit commitment constraints can be imposed based on the injection limits that can be described as:

$$u^{ti} P_{min}^{tijk} \leq p^{tijk} \leq u^{ti} P_{max}^{tijk}. \tag{24}$$

The constraints are setup based on the start-up and shutdown events as:

$$u^{ti} - u^{(t-1)i} = v^{ti} - w^{ti}. \tag{25}$$

The up and downtime of the generators for different time horizons can be written as:

$$\sum_{y=t-\tau_i^+}^{t} v^{yi} \le u^{ti}, \quad \sum_{y=t-\tau_i^-}^{t} w^{yi} \le 1 - u^{ti}. \tag{26}$$

The binary variables are represented as the following constraints:

$$u^{ti} \in \{0,1\}, v^{ti} \in \{0,1\}, w^{ti} \in \{0,1\}. \tag{27}$$

2.5 Modelling the Uncertain Wind Power, Load Demand Conditions And Contingency Scenarios

Wind and load power are modelled as per Figure 1 from the Dalrymple project, Australia [60]. Its pattern for 30 days, along with its mean and confidence intervals are shown in Figure 2. The plot is created using the Seaborn library in Python. The data used for modelling is one-month data sampled at 4-sec intervals. It was then lumped to obtain hourly mean and standard deviation (SD) datasets. The data wrangling is carried out in the Pandas library in Python for missing data removal using previous samples and data reformatting from long stream to hourly interval calculation. Since the optimization approach is considered for 12 hours, the distribution of the wind power is modelled as per the scheme described in Figure 1 to represent the monthly data within this time interval.

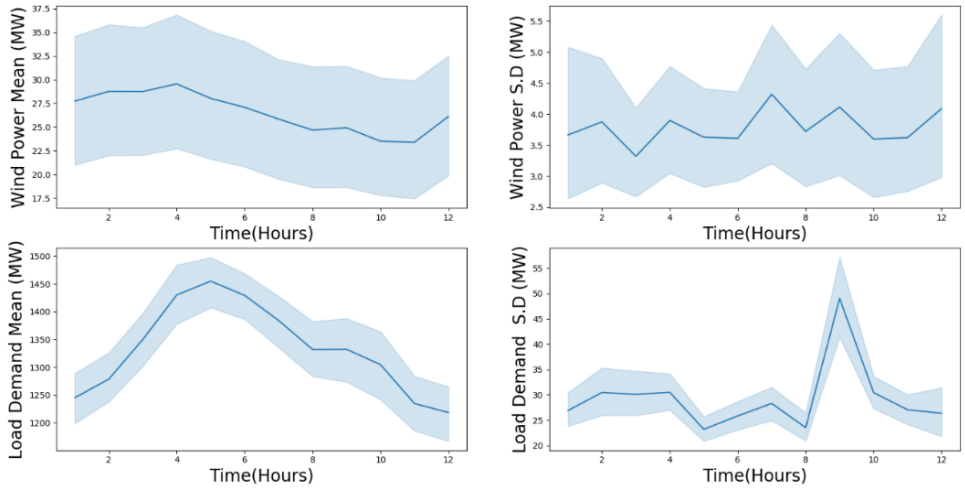

Figure 2. Wind power and load demand mean and standard deviation profiles at various hourly instants considered in the optimization algorithm. Confidence intervals are calculated based on 24×30/12 = 60 samples per hour.

In order to model the hourly characteristics of the data in [60], the data partition is done hourly. The standard deviation of the samples in the given hour is obtained. The hourly standard deviation and the mean of hourly wind power and load demand are uncorrelated as per the multivariate plot shown in Figure 3. The hourly standard deviation data is fitted with a chosen probability distribution. According to the data, the lognormal distribution provides the best fit for the hourly deviation data whose probability distribution function is given as:

$$\mathrm{WIND}_{\mathrm{SD}}(x) = \frac{1}{x\sigma_1\sqrt{2\pi}} \exp\left(-\frac{(\ln x - \mu_1)^2}{2\sigma_1^2}\right) \tag{28}$$

Here, x represents the samples from the above distribution μ_1 and σ_1 represents parameters of the distribution signifying expected mean and standard deviation of the natural logarithm of variable x. The `distributionFitter()` function in Statistics and Machine Learning Toolbox of Matlab is used to find the parameter value with maximum log-likelihood value. The estimated parameters of this density are $\mu_1 = -2.865$

and $\sigma_1 = 0.983$. The samples for the Monte Carlo simulation were generated using the function `random()` in the Statistics and Machine Learning Toolbox in Matlab. The samples are generated, incorporating the inverse transform sampling method. The inverse sampling method draws random numbers from probability distribution function (pdf) defined in (28) with specified parameters and its cumulative distribution function (CDF).

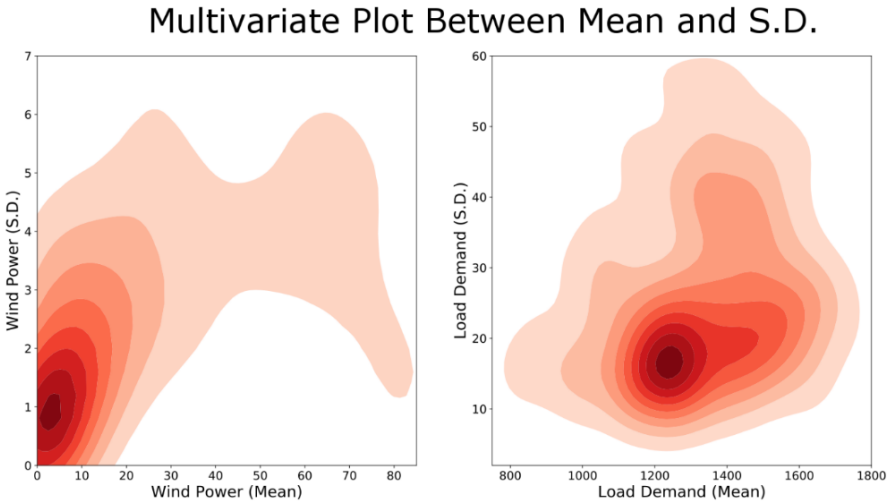

Figure 3. Correlation plot between the mean and standard deviation of load demand and wind power. Distributions of wind and load mean and SDs are calculated based on 24×30 = 720 data points.

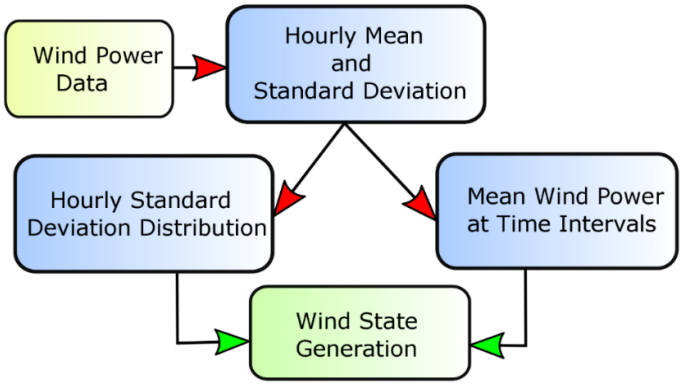

Figure 4. Procedure to generate the wind states from the standard deviation and mean wind power generated from the real data.

The mean wind power value is obtained by calculating the mean value of equally partitioned data as per 12 hours interval. The wind data follow a normal distribution at a particular hour, as given in [61]. Hence three random states are generated from the mean and standard deviations model. It is then quantized as a low, medium, and high wind power scenario, as shown in Figure 4. The MOST solver represents the wind power in per unit (pu). The mathematical relations between the wind states are described in (29).

The prediction error due to the wind follows a normal distribution $\mathcal{N}\left(\mu,\sigma^2\right)$, as given in [61]. Discrete probability values are used to represent continuous probability distribution. Three scenarios of wind power $p_w = \left\{p_{w1}, p_{w2}, p_{w3}\right\}$ are modelled as per the following set of equations:

$$\begin{aligned} &\omega_1 p_{w1} + \omega_2 p_{w2} + \omega_3 p_{w3} = \mu, \\ &\omega_1 p_{w1}^2 + \omega_2 p_{w2}^2 + \omega_3 p_{w3}^2 = \sigma^2 + \mu^2, \end{aligned} \tag{29}$$

where, μ and σ is obtained from the scheme defined in Figure 4.
The wind states following Markovian behaviour, with the stationary distribution $\pi = \left\{\omega_1, \omega_2, \omega_3\right\}$, the following relations hold:

$$\pi\Psi = \pi, \tag{30}$$

where, Ψ represents the transition probability matrix for the states. The vector $\pi = \{\omega_1, \omega_2, \omega_3\}$ is modelled in the simulations from the `asymptotics()` function in the Econometrics toolbox in Matlab. Hence, the vectors obtained in (29) are used as states representing the low, medium, and high power states, as shown in Figure 4.

A similar approach is used for modelling the load power, as shown in Figure 5. The mean and standard deviation is calculated from equally partitioned data. The partitions represent the hourly horizons in the optimization algorithm. It is shown that the mean demand follows a normal distribution whose probability distribution is given as:

$$\text{LOAD}_{\text{MEAN}}(x) = \frac{1}{\sigma_2\sqrt{2\pi}} \exp\left(-\frac{1}{2}\left(\frac{x-\mu_2}{\sigma_2}\right)^2\right), \tag{31}$$

where μ_2 and σ_2 represents the mean and standard deviation of the random variable x considered here. The estimated parameters for this density are given as $\mu_2 = 666.45$ and $\sigma_2 = 105.76$.

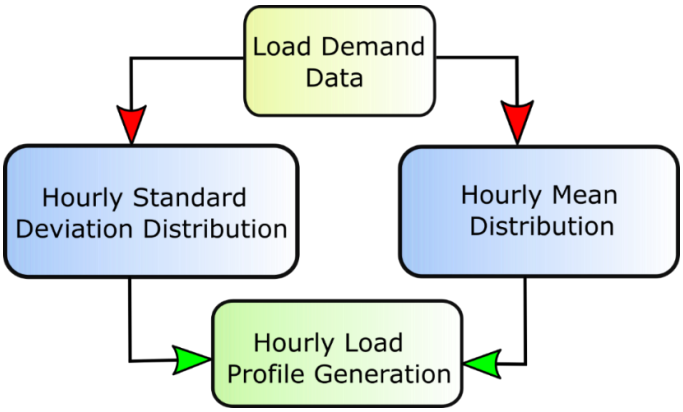

Figure 5. Hourly load profile generation from the hourly standard deviation and mean distribution obtained from the real data.

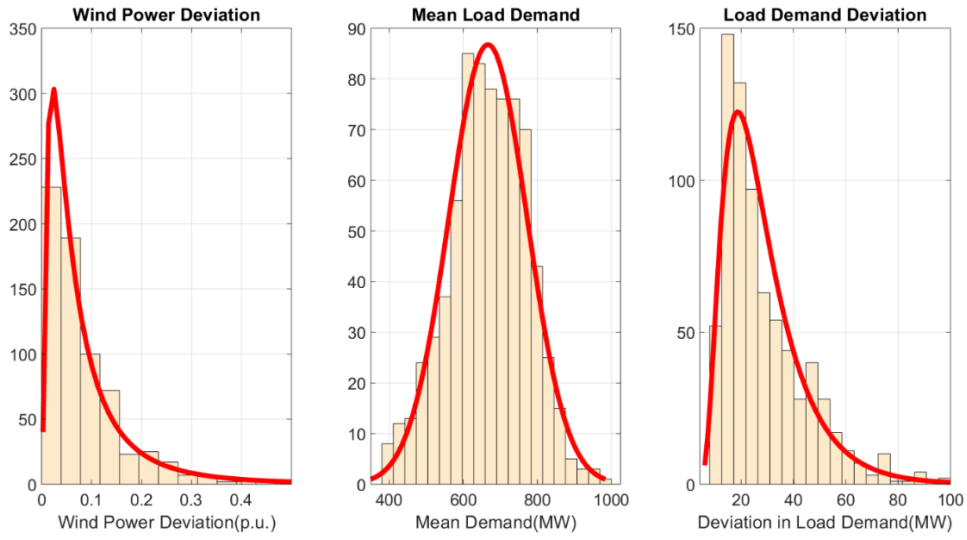

Figure 6. Best fitted probability distributions for the wind power deviation, mean load demand, and load demand deviation to generate Monte Carlo samples for the simulation studies.

The standard deviation of the load demand data follows an inverse Gaussian distribution whose probability distribution is given as:

$$\mathrm{LOAD}_{\mathrm{SD}}(x)=\sqrt{\frac{\lambda}{2\pi x^{3}}}\exp\left[-\frac{\lambda(x-\mu_{3})}{2\mu_{3}^{2}x}\right]. \tag{32}$$

Here the value μ_3 is the mean of random variable x and λ represents the shape parameter. The estimated parameters for this density are $\mu_3 = 14.24$ and $\lambda = 49.48$. The histograms of the probability distribution of the variables used in Monte Carlo simulations are shown in

Figure 6.

Since the optimization problem is a multi-period problem with the known dispatched and storage states. The transition of the given state to any scenario is considered as follows. The probability of operation in period *t*, with no contingency, realized in previous periods is represented as:

$$\gamma^{t}=\sum_{j\in J^{t-1}}\psi^{(t-1)j0}=\sum_{j\in J^{t},k\in K^{tj}}\psi^{tjk}<1,\ \text{for}\ t>1. \tag{33}$$

Let us consider the probability of transitioning to the scenario j_2 in the time t provided that the scenario j_1 was realized at the time $(t-1)$ has a known value $\phi^{tj_2j_1}$. The transition probability at time step *t* is arranged in a probability transition matrix given by:

$$\Phi^{t}=\begin{pmatrix}\phi^{t11} & \cdots & \phi^{t1n_{J^{t-1}}}\\ \vdots & \ddots & \vdots\\ \phi^{tn_{J^{t}}1} & \cdots & \phi^{tn_{J^{t}}n_{J^{t-1}}}\end{pmatrix}. \tag{34}$$

Transition probability matrix, where each scenario at a time step $(t-1)$ can be transitioned to scenarios at *t* is represented as:

$$\begin{bmatrix}\gamma^{t1}\\ \gamma^{t2}\\ \vdots\\ \gamma^{tn_{J^{t}}}\end{bmatrix}=\Phi^{t}\begin{bmatrix}\psi^{(t-1)10}\\ \psi^{(t-1)20}\\ \vdots\\ \psi^{(t-1)n_{J^{t-1}}0}\end{bmatrix}, \tag{35}$$

where,

$$\gamma^{tj}=\sum_{k\in K^{tj}}\psi^{tjk}. \tag{36}$$

Since the sum across *k* of the conditional probabilities of contingencies ψ_0^{tjk} is 1, the values of γ^{tj} are scaled to get the correct state-specific probabilities:

$$\psi^{tjk}=\gamma^{tj}\psi_0^{tjk}. \tag{37}$$

In the case of generator outage contingency, the simulation does not take into account the dependency of the transition probability with the commitment status of the generator unit.

3 NON-PARAMETRIC HYPOTHESIS TESTING

3.1 MULTIVARIATE NORMALITY TEST

It is essential to check the assumptions regarding the underlying distributions of the data. Multivariate Analysis of Variance (MANOVA) is used in [62] for testing the multivariate samples. In the test, it is assumed that the underlying distribution is normal. Multivariate skewness and kurtosis measures are used to find the underlying normality as shown in [63].

Let us consider the random variables $y_1,\ldots,y_m$. For any general multivariate distribution, the following terms can be defined for a sample size of n:

$$\hat{\beta}_{1m}=\frac{1}{n^2}\sum_{i=1}^{n}\sum_{j=1}^{n}g_{ij}^3,\hat{\beta}_{2m}=\frac{1}{n^2}\sum_{i=1}^{n}g_{ii}^2=\frac{1}{n^2}\sum_{i=1}^{n}d_i^4, \tag{38}$$

where, $g_{ij}=\left(y_i-\bar{y}\right)'\mathbf{S}_n^{-1}\left(y_j-\bar{y}\right)$ and $d_i^4=\sqrt{g_{ii}}$. Here $\mathbf{S}_n$ and $\bar{y}$ denotes the covariance matrix and sample mean, respectively. The quantities $\hat{\beta}_{1m}$ and $\hat{\beta}_{2m}$ are the skewness and kurtosis coefficients. When there is a departure from the spherical symmetry, $\hat{\beta}_{1m}$ tends to be close to zero and $\hat{\beta}_{2m}$ tends to be significant for the multivariate normal data as shown in [64]. The hypothesis test is conducted based on Mahalanobis distance g_{ii} and the critical value (κ_1), which is defined by:

$$\kappa_1=n\hat{\beta}_{1m}/6, \tag{39}$$

with $m(m+1)(m+2)/6$ being the degrees of freedom and the critical significance level specified in the test. The above test is performed using the function `mult.norm()` in the *QuantPsyc* package in R [65]. If the hypothesis is accepted within the significance level, then the multivariate extension of ANOVA test (MANOVA) has been performed. Otherwise, non-parametric multivariate testing is performed, which is explained in the next subsection.

3.2 General Non-Parametric Multivariate Test

Non-parametric inference for testing the hypothesis of multivariate samples has been performed, as described in [66]–[68]. The multivariate samples used are of the form $X_{ij}=\left[x_{ij}^{(1)},\ldots,x_{ij}^{(m)}\right]^T$ where $i=1,\ldots,a$ represent the samples to be tested and $j=1,\ldots,n_i$ represent the results from the Monte Carlo samples, $k=1,\ldots,m$ denote the multi-period intervals for optimization. The random vectors are assumed independent with the dependent distribution given as $X_{ij}=\left[x_{ij}^{(1)},\ldots,x_{ij}^{(m)}\right]^T\sim F_i$. F_i can be represented as a degenerate distribution defined as:

$$F_i^{(k)}(x)=\frac{1}{2}\left[P\left(x_{ij}^{(k)}\le x\right)+P\left(x_{ij}^{(k)}\le x\right)\right], \tag{40}$$

where, $P(.)$ represents the probability of the variable *x*. The null hypothesis in terms of distribution functions considering the multivariate hypothesis is given as:

$$H_0:F_1^{(k)}=\cdots=F_A^{(k)}. \tag{41}$$

The alternative hypothesis is that the *F* statistic is unequal between different samples.

The non-parametric statistics generally deals with the rankings of m different variables. The column vector $\mathbf{R}_{ij}=\left(\mathbf{r}_{ij}^{(1)},\ldots,\mathbf{r}_{ij}^{(m)}\right)^T$ consists of the rank of multivariate observations X_{ij}, and the matrix $\mathbf{R}=\left(\mathbf{R}_{11},\cdots,\mathbf{R}_{1n_i},\mathbf{R}_{21},\cdots,\mathbf{R}_{n_a}\right)$ has the ranks for all observations among the variable. The Wilks' Lambda statistic is the commonly used measure for statistical significance due to its flexibility and robustness [68]. The asymptotic results state that either the number of samples A is quite large while the sample size n is fixed or vice versa. $\mathbf{G_1}$ and $\mathbf{H_1}$ are defined as a multivariate version of the residual sum of squares within groups and between groups, respectively [66]. It is defined as:

$$\begin{aligned}\mathbf{G_1}&=\frac{1}{N-A}\sum_{i=1}^{A}\sum_{j=1}^{n_j}\left(\mathbf{R}_{ij}-\bar{\mathbf{R}}_{i\cdot}\right)\left(\mathbf{R}_{ij}-\bar{\mathbf{R}}_{i\cdot}\right)^T,\\ \mathbf{H_1}&=\frac{1}{A-1}\sum_{i=1}^{A}n_i\left(\bar{\mathbf{R}}_{i\cdot}-\bar{\mathbf{R}}_{\cdot\cdot}\right)\left(\bar{\mathbf{R}}_{i\cdot}-\bar{\mathbf{R}}_{\cdot\cdot}\right)^T,\end{aligned} \tag{42}$$

where, $\bar{\mathbf{R}}_{i\cdot}$ represents the mean rank of i^{th} group while $\bar{\mathbf{R}}_{\cdot\cdot}$ represents the overall rank of the groups.

The Wilk's Lambda statistic derived for the asymptotic approximations can be defined using (42) as:

$$T_1 = -\log \frac{\det\left[(N-A)\mathbf{G_1}\right]}{\det\left[(N-A)\mathbf{G_1} + (A-1)\mathbf{H_1}\right]}, \tag{43}$$

where, $N = \sum_{i=1}^{A} n_i, .$

3.3 FINITE SAMPLE APPROXIMATION OF THE MULTIVARIATE SAMPLES

The test statistic described in the previous section is applicable when the multi-period cases or sample sizes are significant. For the total sample size $N \geq 30$, a normal or limiting χ^2 distribution may not describe the actual probability distribution of the test statistic as shown in [68], [69]. The F-approximation works well than the traditional χ^2 (chi-squared) approximation for the smaller sample size. The χ^2 distribution with *d* degrees of freedom is defined as the sum of squares of *d* independent standard normal variables. It is defined as:

$$U = \sum_{i=1}^{d} Z_i^2, \tag{44}$$

where $\{Z_1, ..., Z_r\}$ are independent standard normal variables.

Hence, a random variable having F distribution with parameters d_1 and d_2 is defined as a ratio of two χ^2 variates as given in [70]:

$$F = \frac{U_1 / d_1}{U_2 / d_2}, \tag{45}$$

where,

- U_1 and U_2 have χ^2 distribution d_1 and d_2 are degrees of freedom,
- U_1 and U_2 are independent.

Thus, F approximation of the test statistic of the multivariate samples is defined by:

$$F_\lambda = \left[\left(1-\lambda^{1/t}\right)/\left(\lambda^{1/t}\right)\right]\left(df_2 / df_1\right), \tag{46}$$

where,

$$\begin{aligned} \lambda &= \frac{\det\left[(N-A)\mathbf{G_1}\right]}{\det\left[(N-A)\mathbf{G_1} + (A-1)\mathbf{H_1}\right]}, \\ df_1 &= m(A-1), \\ df_2 &= rt - \left(m(A-1)-2\right)/2, \\ r &= (N-A) - \left(m-(A-1)+1\right)/2. \end{aligned} \tag{47}$$

The value t is defined as:

$$\begin{aligned} &\text{if } m(A-1) = 2, \text{ then } t = 1; \\ &\text{else, } t = \sqrt{\frac{m^2(A-1)^2 - 4}{m^2 + (A-1)^2 - 5}}. \end{aligned} \tag{48}$$

Relative effects have been described in [66] which reflects the non-parametric tests complementing the inferential analysis in the form of probabilities. The statistic derived in (46) can be found out using `nonpartest()` function in the *npmv* package in R as described in [68].

4 NUMERICAL VALIDATION

A 3-bus power system has been considered for the numerical validation. The nominal values for the energy and load devices are shown in Figure 7. The security-constrained stochastic unit commitment problems generally become nonconvex when the system considered is large as stated in [71]. It is mainly due to the assumptions involving the parametric cost of the system. Moreover, the problem also becomes ill-conditioned under different opposing contingency schemes, which leads to numerical inaccuracies. Specific scenarios and contingencies can make the computational procedure formidable for a larger grid [3]. Therefore, it becomes challenging to perform simulations under varied conditions. Thus, a smaller grid can provide a reasonable basis of multivariate analysis based on the contingency conditions of all the power system components. The grid structure in Figure 7 has been adopted from the MATPOWER MOST manual given in [72].

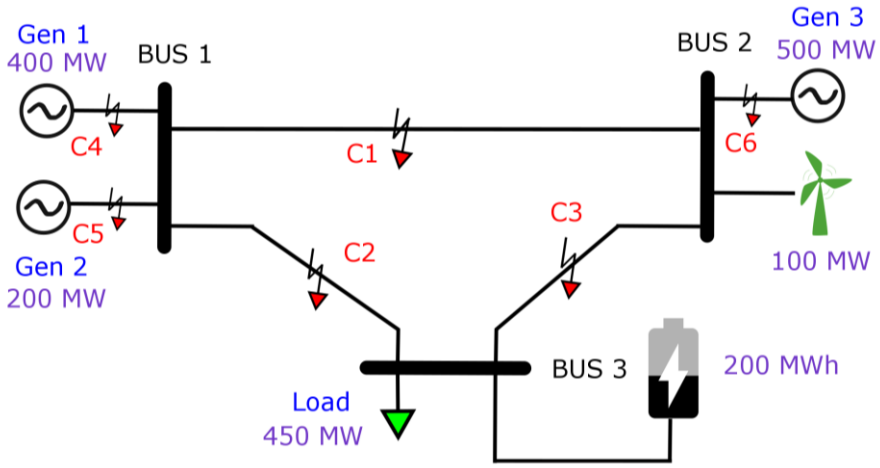

Figure 7. Grid structure for the 3-bus system with generators, wind, load, and battery.

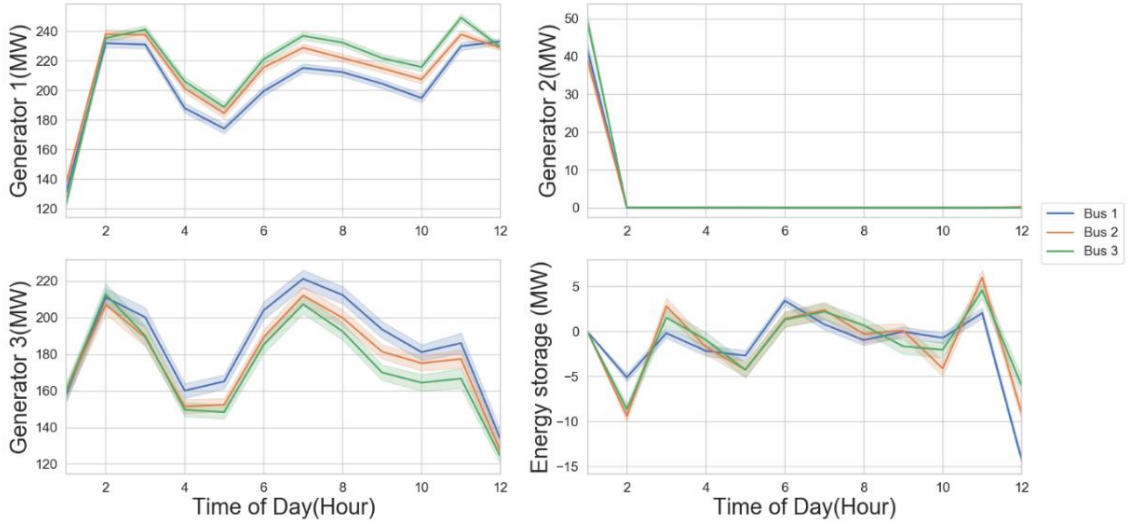

Figure 8. Multi-period optimization results for generator 1, generator 2, and generator 3 and energy storage operations at the base case scenario when the energy storage device is placed at different buses. Confidence intervals are calculated from 1000 independent runs of the stochastic optimization.

The MOST solver was run 1000 times from the random samples of the wind power, load demand, and probability transition matrix, where the *Gurobi* solver has been used to solve the optimization problem. The solver has the feature to solve the problem on a multi-threaded processor. The stochastic optimization algorithm was run on a 64-bit Windows PC Intel Core i5-8500 CPU, 3 GHz processor with six parallel cores. The test grid shown in Figure 7 involves two generators G_1 and G_2 connected to bus 1, which has a nominal rating of 250 MW and 125 MW but maximum peak operational capacity of 400MW and 200 MW, respectively, with the inclusion of locational reserves. G_3 has a nominal rating of 200 MW with a capacity of 500 MW in the presence of locational reserves. Wind power is considered as the stochastic generation input, with 100 MW being considered as the base

value. The dispatchable load is used in the analysis that is curtailable at a specific price with minimum load demand of 450 MW, as shown in Figure 7. Since the sizing problem of energy storage is not considered here, the analysis is performed with an energy capacity of 200 MWh. Maximum charging and discharge rate of 80 MW is considered with an efficiency of 75% as given in [73]. The tripping of all transmission lines and generators are considered as the contingency scenarios shown in Figure 7. The α value (see nomenclature) of 0.06 is assumed in the simulation.

The power flow analysis of the grid structure, considering the nominal ratings of the generators and load, as shown in Figure 7, is performed. The results show that the branch connecting bus-1 to bus-3 is the most critical one as it carries bulk power. The branch connecting bus-1 to bus-2 is the least critical one. The simulation is performed with 1000 samples of wind power and load demand scenarios along with random Markovian transition matrices in each iteration. The decisions for the controllable energy sources without any contingency is shown in Figure 8. In the given figure, the simulations were conducted with the energy storage devices placed on different buses. We observe that G_2 is mostly shut down for most of the time. It is mainly due to its lower rating and peak capacity. We also observe a distinctive pattern in the ESS operational data from Figure 8 when it is placed at different locations of the grid. The optimal conditions of energy dispatch for G1 are higher when the battery is placed at bus-3, the load bus. However, the pattern is reversed in G3, which is connected to the same bus as the wind power source. The dispatch value is higher when the battery source is connected to bus-1, as compared to when it is connected to the load bus-3.

5 RESULTS AND DISCUSSIONS

5.1 ANALYSIS OF THE STORAGE OPERATIONS BASED ON BASE CASE AND CONTINGENCY SCENARIOS

Ensembles of the wind energy and load demand pattern are used from the probability distribution of the mean and standard deviation, which is modelled from the real data, as shown in Figure 6. Based on different values of load demand and wind power from the ensembles, the value of ESS committed will depend upon it. Hence it is expected to obtain charging and discharging patterns for different ensembles. In the case of contingencies, the expected ESS operation changes. In the base case scenario, it is expected to work as a bidirectional device. However, during contingency, ESS will act as a generator to meet the load demand to prevent load shedding. It is interesting to check how the bidirectional nature of ESS changes during different contingencies. Energy storage is expected to provide arbitrage, i.e., charging when the load demand is low and discharging when load demand is high. Regular arbitrage operation can be observed in Figure 8, where the ESS operates in both regions. If it operated in discharge mode, ESS should be able to provide higher power during a contingency.

Table 1: Multivariate normality test results on the energy storage operations data

Storage Location	Contingency Condition	$\hat{\beta}_{1,m}$	$\hat{\beta}_{2,m}$	Critical Distance	*p*-value
Bus-1, Bus-2, Bus-3	-	6.43	19.2	0.6	0
Bus-1	All cases	24	69.8	12.59	0
	C4, C6	1.21	7.38	5.99	0
	C1, C2, C3, C5	21.7	47.2	9.49	0
Bus-2	All cases	2.7	41.6	12.59	0
	C1, C2, C3	1.36	11.3	7.81	0
	C4, C5, C6	0.74	10.6	7.81	0
Bus-3	All cases	2.74	41.3	12.59	0
	C1, C4, C5, C6	1.36	18.8	9.49	0
	C2, C3	0.31	5.19	5.99	0

Similarly, it is expected to provide lower power if it acts in charging mode during the base case scenario since the load demand is expected to be less. Based on this logic, the ESS operational characteristic should ideally follow a linear region when observing the characteristics of base and contingency operations. However, we observe an atypical pattern in Figure 9, Figure 10, and Figure 11. The pattern is mainly due to the absence of the p_{sc} term in s_{Δ}^{tijk} as in (11) during the contingency scenario. The presence of p_{sc} creates a difference in the hourly change in stored energy in different scenarios. The difference in the operation of ESS in the base case scenarios for different contingencies is due to the inter-temporal constraints defined for the operation in [72]. Moreover, this is also due to the presence of γ^{tj} and ψ_{α}^{tjk} in (4) and (5) respectively for total and ramping costs. Due to the presence of these probabilistic parameters referring to the transmission lines and generator outages, the operations during base conditions change during different contingency scenarios. We observe in Figure 8 that the ESS works in charging mode in the final hour. This is mainly because the mean load demand is low, as shown in Figure 2. However, there are certain instances where the ESS works in discharging mode, especially when it is placed on the load bus, as shown in Figure 8.

The stored energy for contingency scenarios is dependent upon the $\beta_3^{ti}, \beta_4^{ti}$ and β_5^{ti}. It is calculated every hourly interval, which varies with α. Hence, these parameters also cause a difference in the minimum and maximum hourly energy discharge as given by (15) and (23) respectively. The data is spread in the linear zone in the first hours of operation. For the higher time, the data-points move along the periphery of the parallelogram. It signifies the nature of the operation of the energy storage devices in the grid at various locations and the type of contingency. Moreover, the peripheral spread in the pattern can also be attributed to the inter-temporal constraints given by (15) and (23). The hourly charging and discharging terms p_{sc}^{t} and p_{sd}^{t} in the base and p_{sd}^{t} contingency cases causes variation in ESS behaviour as explained with the non-parametric multivariate test in the next sections.

5.2 MULTIVARIATE NORMALITY TEST ON THE STORAGE OPERATIONS

The tests described in Section 3.1 can be used to check whether the data follows a multivariate normal distribution. The results obtained after conducting the test are given in Table 1. As we see from Table 1, the *p*-values obtained are all zero, which shows that the underlying data is not normal, hence a non-parametric multivariate test needs to be conducted as described in the next section.

5.3 ANALYSIS OF STORAGE OPERATIONS AT DIFFERENT LOCATIONS IN THE GRID

The data generated from the optimization consists of values obtained for different time horizons and 1000 random samples from wind, load, and transition probability matrix (as described in Section 2.5). The values of m (hourly instants) and n (number of Monte Carlo samples) are 12 and 1000, respectively. The value a depends on the comparison of various contingency conditions. The test statistic F, along with the degrees of freedom df_1 and df_2 are shown in Table 2. We observe from Table 2 that the F statistic is quite high in the case when the storage operation is analysed under the base case scenario as compared to other contingencies which signify that the energy storage operation is more similar under no contingencies as compared to its operation when placed on different buses during several contingencies. When the storage device is placed on bus 1, it operates in extreme regimes, as observed in Figure 9, which signifies that the storage operations are not similar for different contingencies. Moreover, it is also not statistically significant, as shown in Table 2.

5.3.1 ESS Located at Bus 1

We observe from Figure 9 that the operation of the ESS is susceptible to different tripping conditions. The maximum power obtained during contingencies C2, C3, C5 is minimal during later hours of operation. The ESS discharges at low rate during the corresponding charging base states during C1, C2, C3, and C5 contingency. In the case of C4 and C6 contingency, the ESS discharges power to compensate for the contingency of the outage of a higher capacity generator. The ideal case of operation is at the bottom left and top right corner for energy arbitrage, as it has to discharge less amount if it was working in the charging mode in the base case scenario and higher amount if it was working under discharge mode in base case scenario. It is observed partially in the case of all the contingencies except C4 and C6. It shows that the robustness of operation is affected when the energy storage device is placed near the generator bus. It is also observed that, in the case of the C6 contingency scenario, the ESS does not operate for the first few hours, which is not observed in the other contingency situations.

When we observe the discharge conditions of ESS, corresponding to the base case of C1, C2, C3, and C5 contingency, we observe operations mostly during the later hours. However, in the case of C4 and C6 contingency, we observe the ESS operates in discharge mode in the early hours. During the charge conditions of ESS, we observe that the ESS does not operate at full capacity during the contingency situations as compared to its respective base case scenario in the case of C2, C3 and C5 contingency where it works till maximum 12.5 MW, 15MW and 16 MW corresponding to the base case conditions. It operates at maximum capacity in the case of C1, C4, and C6 contingency only when the ESS is charging at a higher rate during the base case scenario.

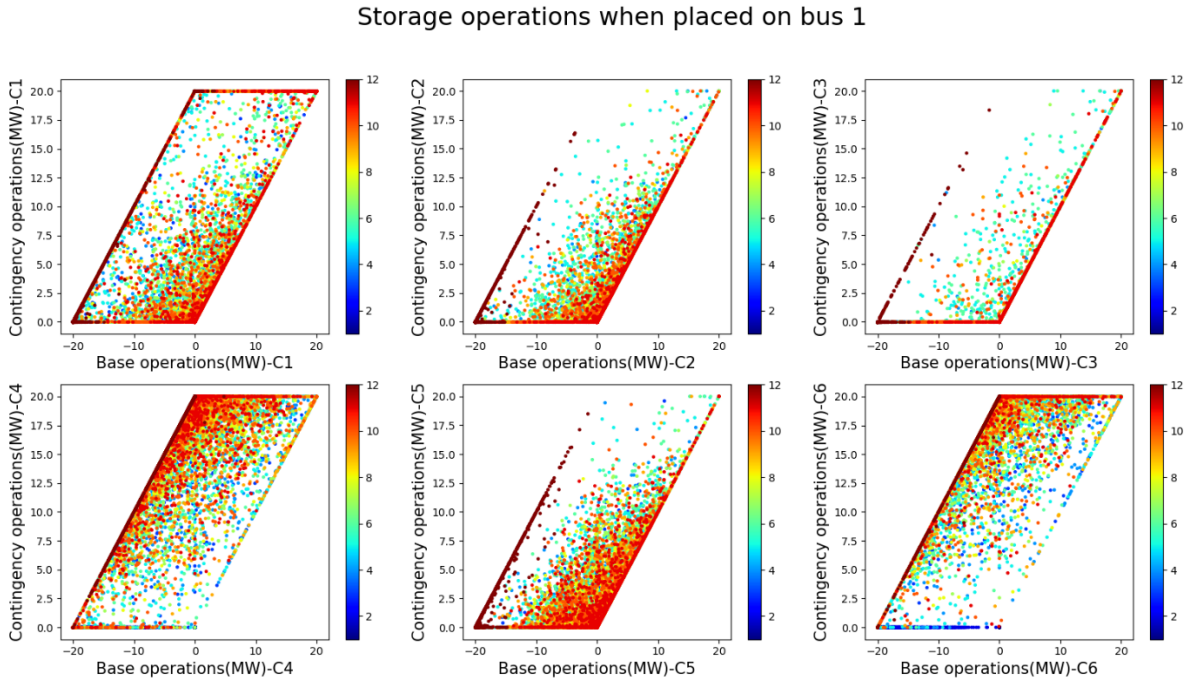

Figure 9. Energy storage operations when placed on bus-1 in the grid under various contingency scenarios for different wind power and load demand ensembles. Colours represent hour of operation between 1-12 hours.

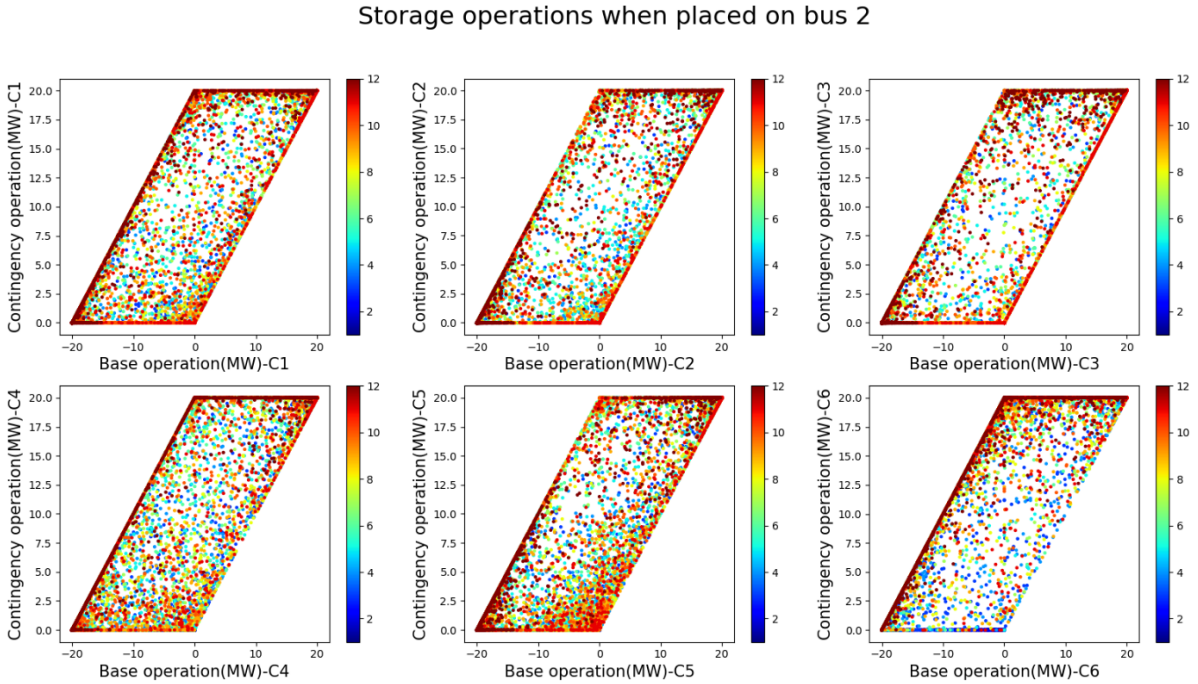

Figure 10. Energy storage operations when placed on bus-2 in the grid under various contingency scenarios. Colours represent hour of operation between 1-12 hours.

We observe a similarity in operational patterns for C1, C2, C3, and C5 contingencies based on the test statistic with lesser degrees of freedom, as shown in Table 2. The operational dissimilarity is observed when lines between bus-1 and bus-2 and G2 is tripped. It is due to the low power flow and the generator capacity. However, it is more sensitive to trips of the lines connecting the load bus. F value of 578 is observed in Table 2, which is significantly higher as compared to other cases due to the outage of generators G1 and G3, which are of higher generation and capacity rating. Hence, the results show that the operation of energy storage is dependent on the tripping of the generator with higher ramping capacity. In addition to this, it is less sensitive to the line trips when placed near the conventional generators with a higher rating.

5.3.2 ESS Located at Bus 2

When the energy storage device is placed on bus-2 near the wind power, we observe a uniform operation across its spectrum as compared to the previous cases shown in Figure 10. It is observed that all ESS would be able to provide higher capacities for all types of contingencies. There are exceptions to the case where we observe a lower rate of ESS operation in case of C2 contingency when the base case charging operation is between 0 to 10 MW during the final hour of the period. However, we do observe a change in ESS operation in the case of C6 contingency. We do not observe a discharging condition during later hours, in the base case scenario. The ESS works mostly in the discharge condition during the base case scenario during the initial hours of operation. We also observe a limit in the maximum discharge during C2 and C5 contingency in the later hours of operation.

However, the F-statistic is lower as compared to the previous location, as shown in Table 2. It indicates a lesser overall similarity in operation. Higher F-statistics in the cases of C4, C5, and C6 contingency are observed in Table 2, which indicates similarity in storage operation in case of generator trips as compared to the line trips. We observe more uniform spread in the data in case of C1 contingency, as compared to C3, which signifies that the modes of operation are more dependent on the tripping of the line connecting the storage to the load as compared to the line not connected between the loads when it is connected.

Table 2: Results of non-parametric multivariate test for storage operations on various grid locations and contingency scenarios

Storage Location	Contingency Condition	Test Statistic (F)	Degrees of Freedom (df_1)	Degrees of Freedom (df_2)	p-value
Bus-1, Bus-2, Bus-3	-	734.319	33	212084.7	0
Bus 1	All cases	373.364	66	64124.67	0
	C4, C6	578.988	22	23974	0
	C1, C2, C3, C5	372.736	44	45853.57	0
Bus 2	All cases	238.755	66	64124.67	0
	C1, C2, C3	182.738	33	35313.67	0
	C4, C5, C6	406.132	33	35313.67	0
Bus 3	All cases	229.655	66	64124.67	0
	C1, C4, C5, C6	196.135	44	45853.57	0
	C2, C3	498.661	22	23974	0

5.3.3 ESS Located at Bus 3

When the energy storage is placed in bus 3, we observe that the ESS works in discharge mode during the base case scenarios. However, it operates mostly in charging mode during the later hours of operation in case of C2 and C3 contingency for base case scenarios. It works on the ideal mode providing optimal energy arbitrage for all

the contingency cases. There is a limit in power provided during the later hours in the case of C5 and C6 contingency. During C2 and C3 contingency, the ESS is not operating in discharge mode for the base case scenario. ESS operates between 15 to 20 MW in case of contingency scenario corresponding to the base case operation during C1, C4, C5, and C6 contingency. Non-operation of the ESS in discharge mode during the base case scenarios proves that the operation of ESS is susceptible to the line trips connecting the load to the generator sources. The uncertainty and the fluctuation of the load demand are reflected in the ESS operations.

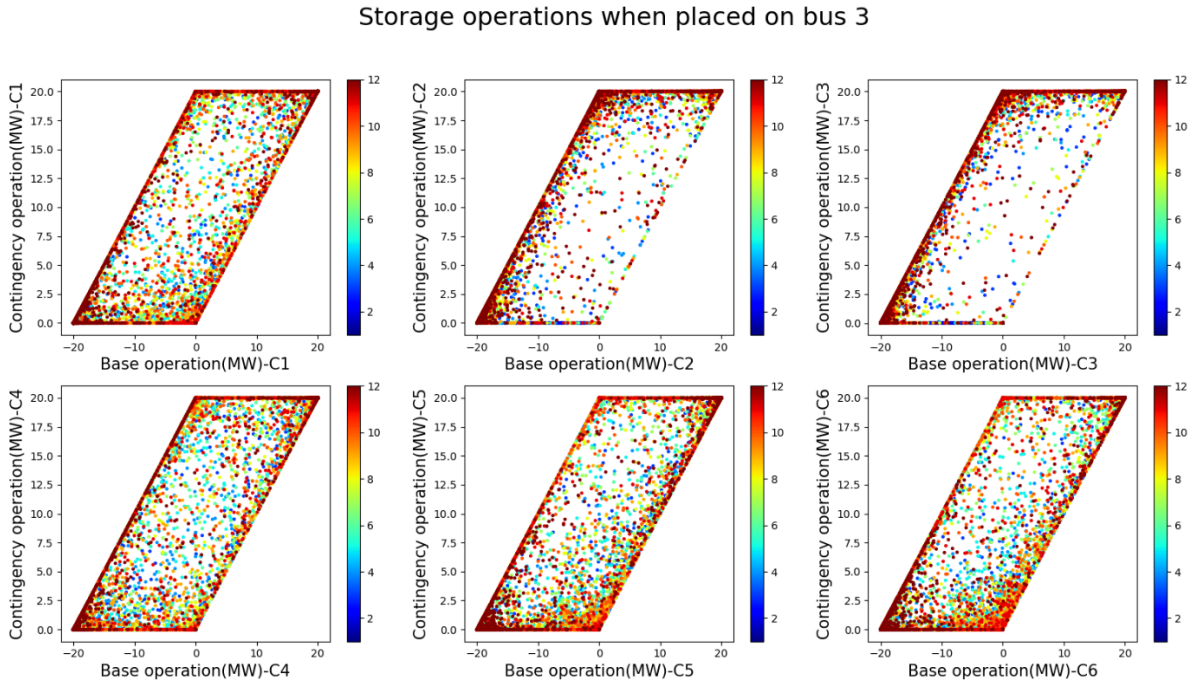

Figure 11: Energy storage operations when placed on bus-3 in the grid under various contingency scenarios. Colours represent hour of operation between 1-12 hours.

Hence, the results show that the operation of the energy storage device is uniform when connected near the stochastic wind energy source as the operations are similar during generator trips. When the energy storage device is connected near the load on bus-3, we see less variation of its operation as compared to the previous cases. The overall F-statistic is similar to the one when the storage device was placed near the wind source. However, in Figure 11, we observe a substantial similarity in operation when the line connecting the load to the generation source trips due to a higher F-statistic in Table 2. There is more dissimilarity in operations in the case of generator trips. Thus, it is evident that the ESS operation, when placed near the load bus, is quite sensitive to trips in the power lines, connecting the bus to the generation source.

The analytics for ESS placement are always better when performed on a smaller grid as done in [25], where the respective net value is compared for different locations in the grid. When, ESS is located near the controlled generation source, it works in extreme modes with lower sensitivity to individual line trips and higher sensitivity to the tripping of generators, especially with high ramping capacity. Uniformity in energy storage operations is observed when ESS is placed in bus 2, near the stochastic renewable energy source. In addition to this, capacity of the ESS is enhanced to provide power during the respective charging and discharging modes in the base case. When the energy storage device is located near the load bus, it is less sensitive to the generator trips and highly sensitive to the tripping of lines connecting the load bus to the generators. However, the operation is not much affected, when the transmission lines, which are not connected to the loads, is tripped. Therefore, the ESS operation is more robust in case of operational contingencies when it is placed near stochastic energy source.

6 CONCLUSION

We demonstrate here a multivariate statistical analysis of energy storage operations during several grid contingency scenarios. We have considered grid operational data obtained from Monte Carlo simulations of a security-constrained stochastic unit commitment algorithm described in [3] with wind power and load demand being random variables. The probability distribution of wind power and load demand scenarios were estimated

from real data. Non-parametric multivariate tests were conducted on the energy storage operations data under the base and several contingency scenarios. The significant research findings of this paper can be summarised as:

- When an energy storage device is located near the controlled generation source, it works in extreme modes with lower sensitivity to individual line trips and higher sensitivity to the tripping of generators, especially with high ramping capacity.
- When the energy storage device is located near the load bus, it is less sensitive to the generator trips and highly sensitive to the tripping of lines connecting the load bus to the generators.
- When the energy storage device is located near the stochastic renewable energy source, the operation is uniform with more similarity due to the generator trips and is recommended for placement.
- The energy storage operation is invariant to the trips of the lines, not connecting to the loads irrespective of its position in the grid.

Future works may be focussed on extending the operational analytics of other components of smart grids, e.g. generators and curtailable loads, and validating them on larger grid models while exploring computational scalability.

ACKNOWLEDGMENT

SD was partially supported by the ESIF ERDF Cornwall New Energy (CNE), Project number 05R16P00282.

REFERENCES

[1] W. F. Pickard and D. Abbott, "Addressing the intermittency challenge: Massive energy storage in a sustainable future," *Proceedings of the IEEE*, vol. 100, no. 2, p. 317, 2012.

[2] D. H. Doughty, P. C. Butler, A. A. Akhil, N. H. Clark, and J. D. Boyes, "Batteries for large-scale stationary electrical energy storage," *The Electrochemical Society Interface*, vol. 19, no. 3, pp. 49–53, 2010.

[3] C. E. Murillo-Sánchez, R. D. Zimmerman, C. L. Anderson, and R. J. Thomas, "Secure planning and operations of systems with stochastic sources, energy storage, and active demand," *IEEE Transactions on Smart Grid*, vol. 4, no. 4, pp. 2220–2229, 2013.

[4] D. Pozo, J. Contreras, and E. E. Sauma, "Unit commitment with ideal and generic energy storage units," *IEEE Transactions on Power Systems*, vol. 29, no. 6, pp. 2974–2984, 2014.

[5] P. Denholm, E. Ela, B. Kirby, and M. Milligan, "Role of energy storage with renewable electricity generation," No. NREL/TP-6A2-47187. National Renewable Energy Lab (NREL), Golden, CO (United States),2010.

[6] M. Aneke and M. Wang, "Energy storage technologies and real life applications-A state of the art review," *Applied Energy*, vol. 179, pp. 350–377, 2016.

[7] S. Chu and A. Majumdar, "Opportunities and challenges for a sustainable energy future," *Nature*, vol. 488, no. 7411, pp. 294–303, 2012.

[8] G. Osório, E. Rodrigues, J. Lujano-Rojas, J. Matias, and J. Catalão, "New control strategy for the weekly scheduling of insular power systems with a battery energy storage system," *Applied Energy*, vol. 154, pp. 459–470, 2015.

[9] L. F. Grisales, A. Grajales, O. D. Montoya, R. A. Hincapie, M. Granada, and C. A. Castro, "Optimal location, sizing and operation of energy storage in distribution systems using multi-objective approach," *IEEE Latin America Transactions*, vol. 15, no. 6, pp. 1084–1090, 2017.

[10] J. Sardi, N. Mithulananthan, M. Gallagher, and D. Q. Hung, "Multiple community energy storage planning in distribution networks using a cost-benefit analysis," *Applied Energy*, vol. 190, pp. 453–463, 2017.

[11] L. A. Wong, V. K. Ramachandaramurthy, P. Taylor, J. Ekanayake, S. L. Walker, and S. Padmanaban, "Review on the optimal placement, sizing and control of an energy storage system in the distribution network," *Journal of Energy Storage*, vol. 21, pp. 489–504, 2019.

[12] Y. Li, B. Feng, G. Li, J. Qi, D. Zhao, and Y. Mu, "Optimal distributed generation planning in active distribution networks considering integration of energy storage," *Applied Energy*, vol. 210, pp. 1073–1081, 2018.

[13] H. Saboori and R. Hemmati, "Maximizing DISCO profit in active distribution networks by optimal planning of energy storage systems and distributed generators," *Renewable and Sustainable Energy Reviews*, vol. 71, pp. 365–372, 2017.

[14] T. K. Brekken, A. Yokochi, A. Von Jouanne, Z. Z. Yen, H. M. Hapke, and D. A. Halamay, "Optimal energy storage sizing and control for wind power applications," *IEEE Transactions on Sustainable Energy*, vol. 2, no. 1, pp. 69–77, 2010.

[15] Y. Zheng, Z. Y. Dong, F. J. Luo, K. Meng, J. Qiu, and K. P. Wong, "Optimal allocation of energy storage system for risk mitigation of DISCOs with high renewable penetrations," *IEEE Transactions on Power Systems*, vol. 29, no. 1, pp. 212–220, 2013.
[16] M. Nick, R. Cherkaoui, and M. Paolone, "Optimal allocation of dispersed energy storage systems in active distribution networks for energy balance and grid support," *IEEE Transactions on Power Systems*, vol. 29, no. 5, pp. 2300–2310, 2014.
[17] R. Fernández-Blanco, Y. Dvorkin, B. Xu, Y. Wang, and D. S. Kirschen, "Optimal energy storage siting and sizing: A WECC case study," *IEEE transactions on Sustainable Energy*, vol. 8, no. 2, pp. 733–743, 2016.
[18] L. Grisales-Noreña, O. D. Montoya, and W. Gil-González, "Integration of energy storage systems in AC distribution networks: Optimal location, selecting, and operation approach based on genetic algorithms," *Journal of Energy Storage*, vol. 25, p. 100891, 2019.
[19] D. Miao and S. Hossain, "Improved gray wolf optimization algorithm for solving placement and sizing of electrical energy storage system in micro-grids," *ISA Transactions*, vol. 102, pp. 376-387, 2020.
[20] M. R. Jannesar, A. Sedighi, M. Savaghebi, and J. M. Guerrero, "Optimal placement, sizing, and daily charge/discharge of battery energy storage in low voltage distribution network with high photovoltaic penetration," *Applied Energy*, vol. 226, pp. 957–966, 2018.
[21] J. Iria, M. Heleno, and G. Cardoso, "Optimal sizing and placement of energy storage systems and on-load tap changer transformers in distribution networks," *Applied Energy*, vol. 250, pp. 1147–1157, 2019.
[22] R. Johnson, M. Mayfield, and S. Beck, "Optimal placement, sizing, and dispatch of multiple BES systems on UK low voltage residential networks," *Journal of Energy Storage*, vol. 17, pp. 272–286, 2018.
[23] L. A. Wong, V. K. Ramachandaramurthy, S. L. Walker, P. Taylor, and M. J. Sanjari, "Optimal placement and sizing of battery energy storage system for losses reduction using whale optimization algorithm," *Journal of Energy Storage*, vol. 26, p. 100892, 2019.
[24] Y. Wang and S. Boyd, "Fast model predictive control using online optimization," *IEEE Transactions on Control Systems Technology*, vol. 18, no. 2, pp. 267–278, 2009.
[25] O. Adeodu and D. J. Chmielewski, "A two-stage procedure for the optimal sizing and placement of grid-level energy storage," *Computers & Chemical Engineering*, vol. 114, pp. 265–272, 2018.
[26] P. Fortenbacher, A. Ulbig, and G. Andersson, "Optimal placement and sizing of distributed battery storage in low voltage grids using receding horizon control strategies," *IEEE Transactions on Power Systems*, vol. 33, no. 3, pp. 2383–2394, 2017.
[27] K. Baker, G. Hug, and X. Li, "Energy storage sizing taking into account forecast uncertainties and receding horizon operation," *IEEE Transactions on Sustainable Energy*, vol. 8, no. 1, pp. 331–340, 2016.
[28] C. K. Das, O. Bass, T. S. Mahmoud, G. Kothapalli, M. A. Masoum, and N. Mousavi, "An optimal allocation and sizing strategy of distributed energy storage systems to improve performance of distribution networks," *Journal of Energy Storage*, vol. 26, p. 100847, 2019.
[29] H. Golpira, A. Atarodi, S. Amini, A. R. Messina, B. Francois, and H. Bevrani, "Optimal Energy Storage System-Based Virtual Inertia Placement: A Frequency Stability Point of View," *IEEE Transactions on Power Systems*, 2020.
[30] M. Bucciarelli, S. Paoletti, and A. Vicino, "Optimal sizing of energy storage systems under uncertain demand and generation," *Applied Energy*, vol. 225, pp. 611–621, 2018.
[31] A. Giannitrapani, S. Paoletti, A. Vicino, and D. Zarrilli, "Optimal allocation of energy storage systems for voltage control in LV distribution networks," *IEEE Transactions on Smart Grid*, vol. 8, no. 6, pp. 2859–2870, 2016.
[32] Y. Zhu, C. Liu, K. Sun, D. Shi, and Z. Wang, "Optimization of battery energy storage to improve power system oscillation damping," *IEEE Transactions on Sustainable Energy*, vol. 10, no. 3, pp. 1015–1024, 2018.
[33] Q. Sun, B. Huang, D. Li, D. Ma, and Y. Zhang, "Optimal placement of energy storage devices in microgrids via structure preserving energy function," *IEEE Transactions on Industrial Informatics*, vol. 12, no. 3, pp. 1166–1179, 2016.
[34] Y. Zhang, S. Ren, Z. Y. Dong, Y. Xu, K. Meng, and Y. Zheng, "Optimal placement of battery energy storage in distribution networks considering conservation voltage reduction and stochastic load composition," *IET Generation, Transmission & Distribution*, vol. 11, no. 15, pp. 3862–3870, 2017.
[35] M. Y. Suberu, M. W. Mustafa, and N. Bashir, "Energy storage systems for renewable energy power sector integration and mitigation of intermittency," *Renewable and Sustainable Energy Reviews*, vol. 35, pp. 499–514, 2014.
[36] A. Gallo, J. Simões-Moreira, H. Costa, M. Santos, and E. M. dos Santos, "Energy storage in the energy transition context: A technology review," *Renewable and Sustainable Energy Reviews*, vol. 65, pp. 800–822, 2016.
[37] H. Zhao, Q. Wu, S. Hu, H. Xu, and C. N. Rasmussen, "Review of energy storage system for wind power integration support," *Applied Energy*, vol. 137, pp. 545–553, 2015.

[38] N. S. Wade, P. Taylor, P. Lang, and P. Jones, "Evaluating the benefits of an electrical energy storage system in a future smart grid," *Energy Policy*, vol. 38, no. 11, pp. 7180–7188, 2010.
[39] A. Monticelli, M. Pereira, and S. Granville, "Security-constrained optimal power flow with post-contingency corrective rescheduling," *IEEE Transactions on Power Systems*, vol. 2, no. 1, pp. 175–180, 1987.
[40] Y. Fu, M., Shahidehpour, and Z. Li, "AC contingency dispatch based on security-constrained unit commitment," *IEEE Transactions on Power Systems*, vol. 21, no. 2, pp. 897–908, 2006.
[41] L. Wu, M. Shahidehpour, and T. Li, "Stochastic security-constrained unit commitment," *IEEE Transactions on Power Systems*, vol. 22, no. 2, pp. 800–811, 2007.
[42] J. Wang, M. Shahidehpour, and Z. Li, "Security-constrained unit commitment with volatile wind power generation," *IEEE Transactions on Power Systems*, vol. 23, no. 3, pp. 1319–1327, 2008.
[43] J. D. Lyon, M. Zhang, and K. W. Hedman, "Capacity response sets for security-constrained unit commitment with wind uncertainty," *Electric Power Systems Research*, vol. 136, pp. 21–30, 2016.
[44] S. Naghdalian, T. Amraee, S. Kamali, and F. Capitanescu, "Stochastic Network-Constrained Unit Commitment to Determine Flexible Ramp Reserve for Handling Wind Power and Demand Uncertainties," *IEEE Transactions on Industrial Informatics*, vol. 16, no. 7, pp. 4580–4591, 2019.
[45] A. Ahmadi, A. E. Nezhad, and B. Hredzak, "Security-constrained unit commitment in presence of lithium-ion battery storage units using information-gap decision theory," *IEEE Transactions on Industrial Informatics*, vol. 15, no. 1, pp. 148–157, 2018.
[46] Z. Zhang, Y. Chen, X. Liu, and W. Wang, "Two-stage robust security-constrained unit commitment model considering time autocorrelation of wind/load prediction error and outage contingency probability of units," *IEEE Access*, vol. 7, pp. 25398–25408, 2019.
[47] M. Sheikh, J. Aghaei, A. Letafat, M. Rajabdorri, T. Niknam, M. Shafie-Khah, and J. P. Catalão, "Security-constrained unit commitment problem with transmission switching reliability and dynamic thermal line rating," *IEEE Systems Journal*, vol. 13, no. 4, pp. 3933–3943, 2019.
[48] Y. Wen, C. Guo, H. Pandzic, and D. S. Kirschen, "Enhanced security-constrained unit commitment with emerging utility-scale energy storage," *IEEE Transactions on Power Systems*, vol. 31, no. 1, pp. 652–662, 2015.
[49] H. Daneshi and A. Srivastava, "Security-constrained unit commitment with wind generation and compressed air energy storage," *IET Generation, Transmission & Distribution*, vol. 6, no. 2, pp. 167–175, 2012.
[50] A. A. Salimi, A. Karimi, and Y. Noorizadeh, "Simultaneous operation of wind and pumped storage hydropower plants in a linearized security-constrained unit commitment model for high wind energy penetration," *Journal of Energy Storage*, vol. 22, pp. 318–330, 2019.
[51] W. Gan, X. Ai, J. Fang, M. Yan, W. Yao, W. Zuo, and J. Wen, "Security constrained co-planning of transmission expansion and energy storage," *Applied Energy*, vol. 239, pp. 383–394, 2019.
[52] P. M. de Quevedo, J. Contreras, M. J. Rider, and J. Allahdadian, "Contingency assessment and network reconfiguration in distribution grids including wind power and energy storage," *IEEE Transactions on Sustainable Energy*, vol. 6, no. 4, pp. 1524–1533, 2015.
[53] V. Guerrero-Mestre, Y. Dvorkin, R. Fernández-Blanco, M. A. Ortega-Vazquez, and J. Contreras, "Incorporating energy storage into probabilistic security-constrained unit commitment," *IET Generation, Transmission & Distribution*, vol. 12, no. 18, pp. 4206–4215, 2018.
[54] R. Charo, A.-S. Maite, and M. Guillermo, "Self-regulation of learning and MOOC retention," *Computers in Human Behavior*, p. 106423, 2020.
[55] F. Becker, R. A. Eser, P. Hoelzmann, and B. Schuett, "The environmental impact of ancient iron mining and smelting on Elba Island, Italy-A geochemical soil survey of the Magazzini site," *Journal of Geochemical Exploration*, vol. 205, p. 106307, 2019.
[56] P. Karpinski, J. Samochowiec, M. M. Skasiadek, L. Laczmanski, and B. Misiak, "Analysis of global gene expression at seven brain regions of patients with schizophrenia," *Schizophrenia Research*, 2020.
[57] W. Senker, H. Stefanits, M. Gmeiner, W. Trutschnig, I. Weinfurter, and A. Gruber, "Does obesity affect perioperative and postoperative morbidity and complication rates after minimal access spinal technologies in surgery for lumbar degenerative disc disease," *World Neurosurgery*, vol. 111, pp. e374–e385, 2018.
[58] P. G. F. Furtado, T. Hirashima, and Y. Hayashi, "Reducing cognitive load during closed concept map construction and consequences on reading comprehension and retention," *IEEE Transactions on Learning Technologies*, vol. 12, no. 3, pp. 402–412, 2018.
[59] R. D. Zimmerman and C. E. Murillo-Sanchez, "Matpower 4.1 user's manual," *Power Systems Engineering Research Center, Cornell University, Ithaca, NY*, 2011.
[60] "DALRYMPLE ESCRI-SA BATTERY PROJECT." [Online]. Available: https://www.escri-sa.com.au/. [Accessed: 17-May-2019]

[61] S. Zhang, Y. Song, Z. Hu, and L. Yao, "Robust optimization method based on scenario analysis for unit commitment considering wind uncertainties," in *2011 IEEE Power and Energy Society General Meeting*, 2011, pp. 1–7.
[62] C. J. Huberty and S. Olejnik, *Applied MANOVA and Discriminant Analysis*, vol. 498. John Wiley & Sons, 2006.
[63] K. V. Mardia, "Measures of multivariate skewness and kurtosis with applications," *Biometrika*, vol. 57, no. 3, pp. 519–530, 1970.
[64] R. Khattree and D. N. Naik, *Applied Multivariate Statistics with SAS software*. SAS Institute Inc., 2018.
[65] T. D. Fletcher, "QuantPsyc: Quantitative Psychology Tools. R package version 1.3, 2008." [Online]. Available: https://cran.r-project.org/web/packages/QuantPsyc/QuantPsyc.pdf
[66] C. Liu, A. C. Bathke, and S. W. Harrar, "A non-parametric version of Wilks' lambda—Asymptotic results and small sample approximations," *Statistics & Probability Letters*, vol. 81, no. 10, pp. 1502–1506, 2011.
[67] A. C. Bathke, S. W. Harrar, and L. V. Madden, "How to compare small multivariate samples using non-parametric tests," *Computational Statistics & Data Analysis*, vol. 52, no. 11, pp. 4951–4965, 2008.
[68] A. R. Ellis, W. W. Burchett, S. W. Harrar, and A. C. Bathke, "Non-parametric inference for multivariate data: the R package npmv," *Journal of Statistical Software*, vol. 76, no. 4, pp. 1–18, 2017.
[69] T. Anderson, *An introduction to multivariate statistical analysis*, 1984.
[70] M. H. DeGroot, *Probability and Statistics (2nd Ed)*. Addison-Wesley., 1986.
[71] J. Cao, W. Du, and H. Wang, "An improved corrective security constrained OPF with distributed energy storage," *IEEE Transactions on Power Systems*, vol. 31, no. 2, pp. 1537–1545, 2015.
[72] R. D. Zimmerman and C. E. Murillo-Sánchez, "Matpower Optimal Scheduling Tool MOST 1.0 User's Manual," *Power Systems Engineering Research Center (PSerc)*, 2016.
[73] K. Divya and J. Ostergaard, "Battery energy storage technology for power systems—An overview," *Electric Power Systems Research*, vol. 79, no. 4, pp. 511–520, 2009.